RSC Advances

REVIEW

View Article Online
View Journal | View Issue

Cite this: *RSC Adv.*, 2024, **14**, 4946

All-inorganic lead halide perovskites for photocatalysis: a review

Yajie Huang, Jiaxing Yu, Zhiyuan Wu, Borui Li and Ming Li *

Nowadays, environmental pollution and the energy crisis are two significant concerns in the world, and photocatalysis is seen as a key solution to these issues. All-inorganic lead halide perovskites have been extensively utilized in photocatalysis and have become one of the most promising materials in recent years. The superior performance of all-inorganic lead halide perovskites distinguish them from other photocatalysts. Since pure lead halide perovskites typically have shortcomings, such as low stability, poor active sites, and ineffective carrier extraction, that restrict their use in photocatalytic reactions, it is crucial to enhance their photocatalytic activity and stability. Huge progress has been made to deal with these critical issues to enhance the effects of all-inorganic lead halide perovskites as efficient photocatalysts in a wide range of applications. In this manuscript, the synthesis methods of all-inorganic lead halide perovskites are discussed, and promising strategies are proposed for superior photocatalytic performance. Moreover, the research progress of photocatalysis applications are summarized; finally, the issues of all-inorganic lead halide perovskite photocatalytic materials at the current state and future research directions are also analyzed and discussed. We hope that this manuscript will provide novel insights to researchers to further promote the research on photocatalysis based on all-inorganic lead halide perovskites.

Received 22nd November 2023
Accepted 11th January 2024

DOI: 10.1039/d3ra07998h

rsc.li/rsc-advances

1 Background and development of perovskite materials

1.1 Non-perovskite photocatalysts and oxide perovskite photocatalysts

Globally, the challenges of the energy crisis and environmental pollution are becoming more severe.[1] An increasing number of studies have investigated the efficient use of solar energy to overcome these problems.[2–4] Among these methods, visible light catalysis technique has demonstrated considerable promise. A wide range of photocatalysts has been extensively studied in photocatalytic processes.

TiO_2 was originally used as a photocatalyst to break down water into H_2 and O_2.[5] Different catalysts have been employed, including metal oxides (ZnO, WO_3, Co_2O, CeO_2),[6–8] metal sulfides (MoS_2, WS_2, Co_3S_4),[9–14] nitrides (C_3N_4, GaN),[15,16] phosphides (InP, Ni_2P, CoP, FeP),[17–26] and carbides (C_3N_4, rGO, MoC).[27–31] Photocatalysts with band gap (E_g) larger than 3 eV, such as TiO_2, ZnO, and MnS, have a fatal flaw: they can only be activated by UV light and cannot respond to a wide range of visible light regions. However, independent photocatalysts with E_g less than 3 eV, such MoS_2, WO_3, and C_3N_4, are impacted by the quick recombination of photogenerated carriers even though they exhibit photocatalytic activity under visible light irradiation. In short, these conventional photocatalysts still have several issues such as poor light absorption,[32] low quantum efficiency,[33–36] high interfacial charge transfer resistance,[37] and rapid photogenerated carrier complexation,[38–41] thus significantly restricting the development and practical applications of photocatalysis. A range of efficient techniques, such as doping, implementing cocatalysts, building heterostructures, as well as controlling the morphology and crystallography, have been employed to conquer the aforementioned drawbacks and enhance the photocatalytic activity (Table 1).

Perovskite materials have drawn considerable attention as suitable photocatalysts. The general chemical formula of perovskites is ABX_3, where A, B, and X represent monovalent cations (La^+, Bi^+, $CH(NH_2)_2^+$, $CH_3NH_3^+$, Cs^+, *etc.*), divalent cations (Pb^{2+}, Mn^{2+}, Co^{2+}, Ti^{2+}, *etc.*), and oxygen, halogen, *etc.* (O, Cl^-, I^-, Br^-, *etc.*), respectively.[42] When X is O, ABO_3 is called an oxide perovskite; organic–inorganic hybrid perovskites generally use $CH_3NH_3^+$ (MA) or $CH(NH_2)_2^+$ (FA) as the A-site cation. When Pb^{2+} is the B-site cation and Cl^-, I^-, Br^- or their mixtures are the halide ions (X), $CsPbX_3$ is called an all-inorganic lead halide perovskite.[43] The three-dimensional structure of a perovskite is formed by connecting the vertex corners of the $(BX_6)^{n-}$ octahedron, which is made up of X^- and B^{2+}, with B^{2+} occupying the middle position within the octahedron. The photocatalytic performance of perovskites will be influenced by its crystal structure. The hybridization of the O 2p orbital of the cation in the crystal structure and the 3d orbital of

College of Forestry, Northeast Forestry University, Harbin 150040, China. E-mail: liming1986@nefu.edu.cn; Tel: +86-451-82192120

Table 1 Comparison and summary of the photocatalytic performance of inorganic halide perovskites and non-perovskites[a]

No.	Sample	Application	Synthesis method	Photocatalytic performance	Ref.
1	Ag/TiO_2	Degradation of MB wastewater	Sol–gel method	Degradation efficiency of MB is 98.86% (5 mg per L MB, 250 min)	49
	$CsPbBr_3$/PMMA	Degradation of MB wastewater	Electrospinning technology	Degradation efficiency of MB is 99.18% (5 mg per L MB, 60 min)	50
2	TiO_2/PCN-224	H_2 production	Vacuum filtration	H_2 production rate (1.88 mmol g^{-1} h^{-1})	51
	$CsPbBr_3$	H_2 production	Hot injection	H_2 evolution rate is 133.3 μmol g^{-1} h^{-1} (saturated HBr aqueous solution)	52
3	$ZnS/ZnIn_2S_4$	CO_2 reduction	Hydrothermal	Acetaldehyde yield 367.63 μmol g^{-1} (selectivity 99.6%)	53
	$Co/CsPbBr_3/TiO_x$	CO_2 reduction	Electrostatic self-assembling	The rate of CO_2 reduction reaches 405.2 μmol g^{-1} h^{-1}	54
4	TiO_2/rGO/Cu_2O	Degradation of antibiotic wastewater	Hummers method	Removal rate of TC is 99.38% (100 mg L^{-1}, 40 min)	55
	$CsPbBr_3$–TiO_2	Degradation of antibiotic wastewater	Solvothermal method	Removal rate of TC is 94% (20 mg L^{-1}, 60 min)	56
5	InP/InPS/ZnS	H_2 evolution	Hot injection	The rate of H_2 production reached 102 μmol mg^{-1} h^{-1}	57
	$CsPbX_3$@ZIF-8	H_2 evolution	Mechanical milling	The rate of H_2 production reached 7.852 μmol g^{-1} h^{-1}	58
6	MoS_2	Heavy metal degradation	Ball milling	Cr(VI) removal rate can reach 98.9% (180 min)	59
	$CsPbI_3$/ZnO	Heavy metal degradation	Hot injection	Degradation efficiency of heavy metal is 52%	60
7	g-C_3N_4/CeO_2	Degradation of RhB wastewater	Calcination and hydrothermal	The RhB degradation rate reached 99.07% (7 mg L^{-1} 60 min)	61
	$CsPbBr_3$/PMMA	Degradation of RhB wastewater	Ball milling	The RhB degradation rate reached 92.2% (10 mg L^{-1} 60 min)	62

[a] MB: methylene blue, PMMA: polymethyl methacrylate, TC: tetracycline hydrochloride, RhB: rhodamine B.

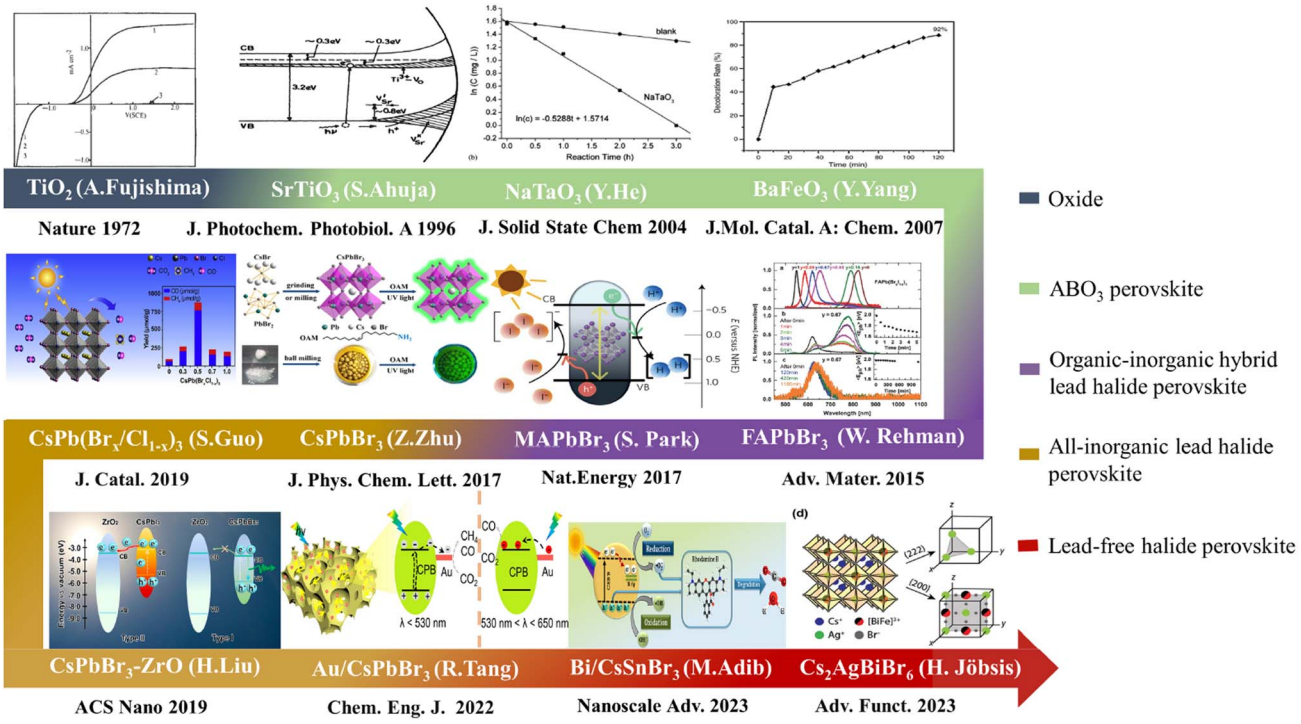

Fig. 1 Development process of perovskite in the photocatalysis field.

Table 2 Summary of typical work of oxide perovskite catalysts (ABO_3) in the field of photocatalysis[a]

Catalysts	Synthesis method	E_g (eV)	Application	Photocatalytic performance	Ref.
$LaFeO_3$/g-C_3N_4/ZnO	Hydrothermal	2.43	Degradation of BP wastewater	Degraded 97.43% of BP (120 min, 20 mg L^{-1}), 90.14% (BPA), 93.68% (PNP), and 92.37% (DCP) (1 h, 20 mg L^{-1})	63
$BaTiO_3$@$SrTiO_3$	Ultrasonic and hydrothermal method	3.23	Water spitting	H_2 evolution rate is 18 μmol g^{-1} min^{-1}	64
$MgFe_2O_4$/Bi_2WO_6	Wet ball milling	2.5	Degradation of TC wastewater	Degradation rate of TC is 95.82% (90 min, 20 mg L^{-1})	65
Ag/$CaZrO_3$	Solid-phase method	5.8	CO_2 reduction	CO production rate (286 μmol g^{-1} h^{-1})	66
Fe–$SrWO_4$	Hydrothermal	3.39	Nitrogen fixation	NH_3 production rate is 385 μmol g^{-1} h^{-1}	67
$LaCoO_3$/MoS_2	Sol–gel, hydrothermal, and ultrasonication method	2.10	Degradation of dye wastewater	Degraded 96% ARS and 90% RhB in 40 min and 80 min, respectively	68
$BiFeO_3$/Bi_2O_3	Auto-combustion method	2.27	Degradation of nitrobenzene	Degraded 100% nitrobenzene	69
$La_{0.9}Sr_{0.1}Fe_{0.8}Co_{0.2}O_3$	Pechini method	2.17	Degradation of dye wastewater	Degraded 98% reactive black 5 (20 ppm, 160 min)	70
$NaTiO_3$/g-C_3N_4	Hydrothermal method	2.3	Degradation of mixed dye wastewater	Degraded 100% mixture of MB and CV in 25 min	71
Pt–$LaMnO_3$	Green solid-state combustion method	2.82	H_2 production	H_2 production rate (40 μmol g^{-1} h^{-1}) (20 vol% methanolic aqueous) solution	72
$BaTiO_3$	Ceramic and complex polymerization methods	3.24	Diclofenac degradation	Presented the DIC removal (61%) (25 mg L^{-1}, 180 min)	73
Bi_2O_4/$NaBiO_3$	Hydrothermal method	1.77	Degradation of MO and BP	Degraded 96.3% MO/BP (20 mg L^{-1}, 60 min)	74
$BiVO_4$/$BaSnO_3$	Facile precipitation method	2.38	Degradation of MB wastewater	With decolorization rate of 94.1% (20 mg L^{-1}, 2 h)	75
TiO_2/$CaTi_4O_9$/$CaTiO_3$	Solvothermal combination with calcination	3.21	H_2 production and Cr(VI) reduction	Produced H_2 at a rate of 25.28 mmol h^{-1} g^{-1} (methanol solution) Cr(VI) reduction rates reached 30.1% (10 mg L^{-1}, 150 min)	76

[a] ARS: alizarin red S, BP: phenol, BPA: bisphenol A, PNP: *p*-nitrophenol, DCP: dichlorophenol, MO: methyl orange.

the transition metal in the (BO_6) octahedron will not only induce lattice distortion but also induce changes in the dipole and electronic structure, thereby affecting the separation of photogenerated carriers, finally leading to perovskites that have unique and variable photocatalytic properties. Furthermore, researchers can specifically build the electronic structure to enhance the stability, charge migration, and light absorption because of a variety of A and B site ions.[44,45] Perovskite materials can also enhance the photocatalytic activity by combining ferroelectric and piezoelectric phenomena.[46,47]

Due to differences in the photoelectric characteristics, different perovskites exhibit varying photocatalytic efficiency. The following characteristics are mostly indicative of the attributes that influence photocatalytic efficiency: (i) light absorption coefficient. The light absorption ability of catalysts affects their photocatalytic performance. The intensity and range of light absorption are crucial markers. (ii) The length of carrier diffusion. Long carrier diffusion length improves photocatalytic efficacy, decreases charge recombination, and helps separate electrons and holes. (iii) Bandgap width. The narrower the band gap of the perovskite, the worse its stability. With an appropriate E_g (2.4–2.7 eV), the all-inorganic perovskite $CsPbX_3$ exhibits excellent stability.

ABO_3 perovskite has been the target of most studies, with impressive findings being obtained in the field of photocatalysis. Mulani *et al.* prepared Ni-doped $LaFe_{0.6}Ni_{0.4}O_3$ through a hydrothermal method to degrade crystal violet (CV), Congo red (CR), and their mixtures under visible light. The degradation efficiencies were 99.2% (210 min), 99.1% (100 min), and 98.4% (70 min), respectively, which were far higher than that of $LaFeO_3$. $LaFe_{0.6}Ni_{0.4}O_3$ degraded CV dye through dealkylation and benzene ring cleavage, while azo bond cleavage and oxidation lead to the production of low molecular weight intermediate products of CR dye.[48] In recent years, oxide perovskites have been rapidly developed in the field of photocatalysis (Fig. 1). Table 2 summarizes the synthesis methods, reaction conditions, and photocatalytic performances of oxide perovskites compared with traditional photocatalysts.

1.2 Oxide perovskite to all-inorganic lead halide perovskites

ABO_3 perovskite exhibited structural flexibility and stability compared with metal oxides; however, it also has shortcomings

Table 3 Summary of all-inorganic lead halide perovskite synthesis methods

No.	All-inorganic lead halide perovskite	Method	Reaction conditions	Ref.
1	$CsPbX_3$ nanocubes (410–530 nm) (X = Cl, Br, I, and mixed systems)	Hot injection method	140–200 °C inert gas protection	115
2	$CsPbBr_3$ nanocrystals (6.8–13.6 nm)	LARP	Room temperature (25 °C) octylphosphonic acid	116
3	$CsPbBr_3$ (film)	Anti-solvent method	Room temperature (varies with season) toluene as an antisolvent	117
4	$CsPbBr_3$ (bulk)	Ball milling method	Ball mill (500 rpm)	112
5	$CsPbI_3$ (8–12 nm)	Ultrasonic method	Room temperature tip ultrasound (power 30 W)	107
6	$CsPbX_3$ (X = Cl/Br, Br and Br/I) nanowires (diameters as small as 2.6 nm)	Solvothermal method	160 °C (high temperature reactor)	113
7	$CsPbBr_3$ quantum dots	Template method	Kaolin as template	118
8	$CsPbBr_3$ nanocrystals (nanoplates, nanocubes)	Microwave synthesis	Microwave reactor 80 °C (nano-plate) 160 °C (nano-cube)	119

Table 4 Advantages and disadvantages of various synthesis methods

Synthesis method	Advantages	Disadvantages	Ref.
Hot injection method	The reaction process is simple and less time-consuming, and the nanocrystals are relatively uniform in morphology and size	Inert gas protection is required during high temperature processes, which will increase the costs in practical applications	134
LARP method	Low cost and simple operation	Nanocrystals have different sizes, poor crystallinity, and low experimental repeatability, making them unsuitable for mass production	135
Anti-solvent method	Small particle size, uniform particle distribution, high dispersion, and controllable morphology	There are many factors that affect the preparation effect of this method (such as the selection and dosage of antisolvent)	136
Ultrasonic method	Low reaction temperature, high purity, small particle size	The purity of synthetic materials differs	129
Solvothemal method	The synthesis conditions are mild, the product purity is high, the crystal grains are fully developed, the particle size is small and evenly distributed, and the morphology is highly controllable	Factors affecting the nucleation process and crystal growth process are difficult to be controlled; highly dependent on equipment	137
Template method	Get good nanoarrays	Templates have the problem of low yield and difficulty in separation. The templates need to be removed, which will destroy the structure of the nanomaterials to a certain extent	138

including large band gap, rapid carrier recombination, small specific surface area, and poor selectivity. Due to the high tunability of band gap, excellent charge mobility, and suitable redox capabilities, organic–inorganic hybrid lead halide perovskites stand out from various materials. Studies have demonstrated that $MAPbI_3$ is consistently and effectively capable of producing H_2 from HI under visible light irradiation, and the solar HI separation efficiency by $MAPbI_3$ is 0.81% when Pt is utilized as a noble catalyst.[77]

Due to their poor stability, organic–inorganic hybrid lead halide perovskites have limited application in photocatalysis. In contrast, all-inorganic lead halide perovskites exhibit highly efficient semiconductor properties. They are employed in various applications, including X-ray fluorescence imaging,[78–82] visible light communication,[83–85] solar cells,[86–89] light-emitting diodes (LEDs),[90–92] lasers,[93,94] photodetectors,[95–97] and photocatalysis. However, most of the previous studies have focused on the optoelectronic properties of all-inorganic lead halide perovskites; a thorough overview of the all-inorganic lead halide perovskites in photocatalysis is urgently required to provide a guide for future research. Herein, all-inorganic lead halide perovskites are summarized in detail with an emphasis on the approaches of synthesis, modification, and applications in photocatalysis. Moreover, the problems and the future development in the field of photocatalysis are summarized and prospected.

2 Synthesis methods of all-inorganic lead halide perovskites

The properties of all-inorganic lead halide perovskites largely depend on their structures, which are directly related to the synthesis methods. Numerous techniques have been investigated to synthesize all-inorganic lead halide perovskites, such

as hot injection,[98–100] room-temperature ligand-assisted deposition,[101–103] microwave synthesis,[104–106] ultrasound synthesis,[107] template method,[108–110] laser irradiation-assisted method,[111] ball milling method,[112] and solvothermal method.[113] These methods can be broadly classified as "bottom-up" or "top-down" depending on the growth process.[114] The two techniques covered in this paper are the hot-injection and ligand-assisted deposition in room-temperature method (LARP), which are widely used for creating all-inorganic lead halide perovskites. The synthesis methods, advantages, and disadvantages of all-inorganic lead halide perovskites are summarized in Tables 3 and 4.

2.1 Hot injection method

The hot-injection method is a typical complex decomposition procedure that involves developing $CsPbX_3$ nanocrystals by completely mixing the PbX_2 precursor material with oleic acid, oleylamine, and octadecene and then rapidly cooling them at high temperatures (140–200 °C). In general, perovskite precursors crystallize into nanoplate-like morphologies at lower reaction temperatures, while they frequently generate cubic nanocrystals at higher reaction temperatures. When the temperature cools down, the size of the perovskite nanocubes also minimizes. The hot injection method can usually obtain dispersed $CsPbX_3$ nanocubes, and the halide composition of the nanocubes can be easily adjusted by changing the proportion of the PbX_2 precursor.

Nedelcu *et al.* firstly achieved the successful hot-injection synthesis of the all-inorganic lead halide perovskite $CsPbX_3$, which also indicated that $CsPbBr_3$ and $CsPbI_3$ had higher photoluminescence quantum yield (PLQY) compared to $CsPbCl_3$.[120] For instance, the PLQY of $CsPbBr_3$ nanocrystals reached 90%[115] (Fig. 2). The hot injection method not only synthesizes pure $CsPbX_3$ but also yields $CsPbX_3$-based composites. Wang *et al.* designed $CsPbBr_3$–CdZnS heterojunctions to photocatalytically reduce CO_2 by the hot-injection method; it was found that the $CsPbBr_3$–CdZnS heterojunction achieved a higher CO yield (55.8 μmol g^{-1} h^{-1}) than that of the pristine $CsPbBr_3$ (13.9 μmol g^{-1} h^{-1}).[121]

The hot-injection method for synthesizing all-inorganic lead halide perovskite nanocrystals has been continuously optimized using different precursors and ligands to achieve the controlment of shape and size as well as better stability over the years.[122] Leng *et al.* successfully synthesized highly stable nanocrystals by designing a "modified hot-injection method" to maximize the number of ligand molecules and lowering the temperature (<40 °C) during precursor mixing to separate the nucleation and growth processes.[123] However, in large-scale production, the inability to adjust the high temperature when combining precursor solutions leads to poor material reproducibility.

2.2 Room-temperature ligand-assisted deposition

Even though the hot-injection method has been widely used to produce all-inorganic perovskite nanocrystals, it is a laborious process that needs extra steps in the synthesis of the Cs-oleate precursor and is typically carried out in an inert environment. LARP is an appropriate remedy for these limitations. Organic ligands and perovskite precursors are dissolved in solvent, and then spontaneous crystallization in a supersaturated state of the crystal can be achieved by lowering the temperature, evaporating the solvent, or adding a lean solvent with a lower solubility of the substance.[124] If crystallization is carried out in the presence of ligands, crystal nucleation and growth can be controlled, which is LARP.

Guvenc *et al.* produced $CsPbX_3$ (X = Br, Cl, I) by LARP; the PLQY of synthesized $CsPbBr_3$ was 85%.[125] By altering the experimental conditions, the LARP method can be used to manufacture all-inorganic lead halide perovskite with various morphologies. Deng *et al.* formed all-inorganic $CsPbX_3$ perovskite in a variety of shapes, including 0D spherical quantum dots, 1D nanorods, and 2D nanoplates[126] (Fig. 3). Zhang *et al.* discovered that stable $CsPbBr_3$ nanocrystals could be manufactured by adding small amounts of water to the reaction mixture, and the PLQY of the $CsPbBr_3$ nanocrystals was 90%.[127]

It is worth noting that perovskite nanocrystals are sensitive to polar solvents; therefore, the synthesized nanocrystals have different sizes, poor crystallinity, and low experimental

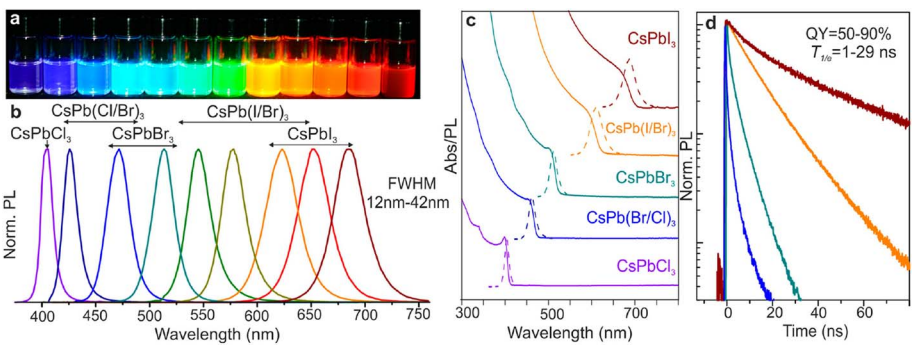

Fig. 2 Colloidal perovskite $CsPbX_3$ (X = Cl, Br, I) exhibit size- and composition-tunable bandgap energies covering the entire visible spectral region with narrow and bright emission: (a) colloidal solutions in toluene under UV lamp (λ = 365 nm); (b) representative PL spectra (λ_{exc} = 400 nm for all but 350 nm for $CsPbCl_3$ samples); (c) typical optical absorption and PL spectra; (d) time-resolved PL decays for all samples shown in (c) except $CsPbCl_3$.[115]

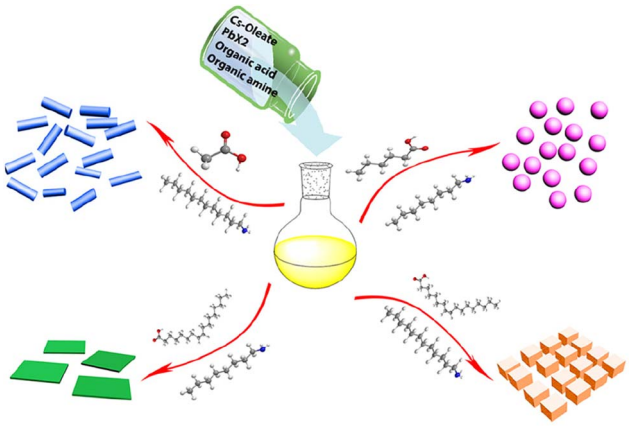

Fig. 3 Schematic illustrating the formation process for different $CsPbX_3$ (X = Cl, Br, I) nanocrystals mediated by organic acid and amine ligands at room temperature. Spherical quantum dots represent hexanoic acid and octylamine; nanocubes represent oleic acid and dodecylamine; nanorods represent acetate acid and dodecylamine; few unit cell-thick nanoplatelets represent oleic acid and octylamine.[126]

repeatability, which are not suitable for large-scale production. To create high-performance all-inorganic lead halide perovskites, the researchers modified the original room-temperature ligand-assisted deposition method. Zeng *et al.* developed a comparable room-temperature supersaturation recrystallization technique to produce $CsPbX_3$ quantum dots.[118] A highly supersaturated state is produced as soon as the halide salt precursor is transferred from a polar (*N*,*N*-dimethylformamide) to a nonpolar solvent (toluene), and the process can be finished without using a protective environment, heating, or injection in only a few seconds. Pan *et al.* investigated the ligand-mediated synthesis of all-inorganic $CsPbBr_3$ perovskite nanocrystals, and the results revealed that CsOAc was a more versatile precursor substance than the commonly used Cs_2CO_3, displaying a greater solubility and a wider temperature.[122]

2.3 Other synthesis methods

2.3.1 Ultrasonic method. The direct sonication of the appropriate precursor solution to create high-quality all-inorganic lead halide perovskite in the presence of organic capping molecules is referred to as the "ultrasonic method". Rao *et al.* used ultrasonic-assisted method to synthesize $CsPbBr_3$ nanocrystals with various shapes and sizes.[128,129]

2.3.2 Ball milling method. Ball milling can be used to produce all-inorganic lead halide perovskites on a large scale,[130] for example, Jiang *et al.* synthesized $CsPbBr_3/Cs_2PbBr_5$ with chemical stability and good photostability by ball milling,[131] showing exceptional stability when exposed to UV light, heat, and water. However, mechanical grinding will result in surface flaws and diminish the photocatalytic effectiveness. Kim *et al.* created a simple two-step ball milling approach to create stable $CsPbBr_3$ [132] and discovered that these materials were more stable after 30 days than those that were thermally synthesized under the same circumstances.

2.3.3 Solvothermal method. The solvothermal method produces scattered nanocubes by loading precursors and ligands into an autoclave lined with Teflon and heating it to a high temperature for a predetermined amount of time. Chen *et al.* reported that high-quality all-inorganic cesium lead halide nanocrystals could be acquired by a simple solvothermal method,[113] and the high-quality $CsPbBr_3$ nanocrystals are ideal for lighting applications.

2.3.4 Microwave synthesis. Pan *et al.* proposed a microwave-assisted strategy to synthesize high-quality $CsPbX_3$ with controllable morphologies (nanocubes, nanoplates, and nanorods),[119] and the prepared $CsPbX_3$ nanocubes showed high PLQY (75%). In addition to the above-mentioned synthetic methods, two or more methods can be combined to synthesize all-inorganic lead halide perovskites. Li *et al.* prepared $CsPbBr_3/SiO_2$ using a template-assisted method[133] and then used high-temperature synthesis by adding a specific quantity of mesoporous silica template to a mixture of CsBr and $PbBr_2$.

3 Modification of all-inorganic lead halide perovskite

Although all-inorganic lead halide perovskites have a great deal of potential for photocatalysis, however, pure halide perovskites typically have some issues, such as low stability, lack of active sites, and ineffective carrier extraction, which restrict the utilization of photocatalytic materials.[139–142] To improve the photocatalytic activity, several techniques have been developed, including ion doping,[143,144] metal loading,[145,146] creation of heterojunctions,[147,148] and anion exchange.[149–152]

3.1 Ion-doping

Doping is a valuable modification strategy that adjusts the chemical structure of the lattice by incorporating some "impurities" to broaden the photoresponse range or enhance the separation of photogenerated carriers.[153–156] To this end, researchers have explored methods of incorporating metal ions at the A-site and B-site. Generally speaking, A-site and B-site doping can be achieved through cation exchange or *in situ* synthesis. Mn^{2+} is the most common dopant ion in the B-site of all-inorganic lead halide perovskites.[157–162] Liu *et al.* prepared Mn^{2+}-doped $CsPbBr_3$ to improve the efficiency of CO_2 reduction[163] (Fig. 4). The results showed that the yields of CO and CH_4 reached 1917 μmol g^{-1} and 82 μmol g^{-1}, which were 14.2 and 1.4 times that of $CsPbBr_3$. In addition, other metal atoms have also been successfully doped into all-inorganic lead-halide perovskites. Patil *et al.* doped $CsPbI_2Br$ nanocrystals with Sr^{2+} to obtain more stable solar cells,[164] and the $CsPb_{0.98}Sr_{0.02}I_2Br$ device maintained more than 85% of its initial efficiency for 100 hours under ambient conditions. Shyamal *et al.* partially substituted Pb^{2+} with Fe^{2+} to create Fe^{2+}-doped $CsPbBr_3$,[165] which was utilized in ethyl acetate/aqueous solution for the photocatalytic reduction of CO_2. Dong *et al.* produced Co^{2+}-doped $CsPbBr_3/Cs_4PbBr_6$ for CO_2 reduction with 1835 mol per g CO_2 yield.[166] All-inorganic lead-halide perovskites are also doped with new ions. In addition to equivalent doping,

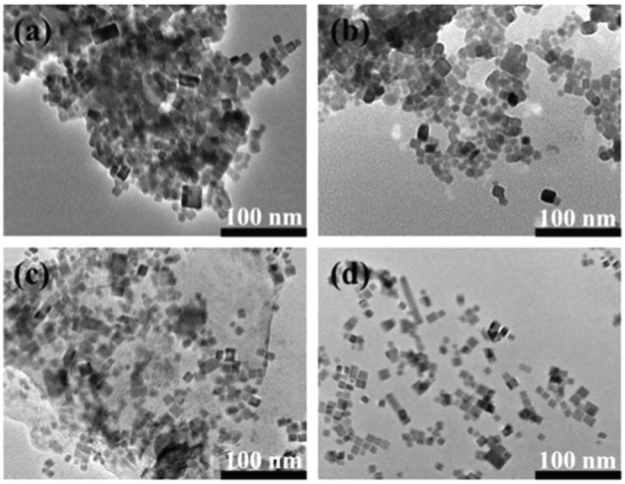

Fig. 4 TEM images of Mn-doped $CsPb(Br/Cl)_3$ mixed-halide perovskites (a) sample 1: the ratio of $PbBr_2/MnCl_2$ is 4 : 1, (b) sample 2: the ratio of $PbBr_2/MnCl_2$ is 2 : 1, (c) sample 3: the ratio of $PbBr_2/MnCl_2$ is 2 : 3, (d) sample 4: the ratio of $PbBr_2/MnCl_2$ is 3 : 7.[163]

heterovalent ions can also be introduced. Zhou *et al.* stabilized $CsPbBr_3$ by co-doping Na^+, and the results showed that co-doping metal ions significantly improved the thermal stability and optical properties of quantum dots.[167] Using calculations based on density functional theory, Wang *et al.* investigated how Bi^{3+} doping affected the structural,[168] electrical, and optical characteristics of $CsPbBr_3$, and the results revealed that Bi^{3+} doping can improve the stability.

Studies on A-site doping are becoming increasingly prevalent. Ru^+ and K^+ are a couple of alkali metal ions that have drawn increased interest as possible dopants. These dopants can be applied to boost the photoluminescence efficiency and stability of perovskite nanocrystals. For example, Huang *et al.* created K–$CsPbBr_3$ nanocrystals that maintained 97.9% of their initial intensity after 30 hours.[169] Ouaaka *et al.* assessed the electrical, optical, thermoelectric, and elastic characteristics of Rb-doped $CsPbBr_3$ by density functional theory. The findings demonstrated that $Rb_xCs_{1-x}PbBr_3$ had excellent ultraviolet absorption capabilities, a low range of E_g, and enhanced thermal–electrical conductivity.[170]

In brief, ion doping has been thoroughly investigated to modify the electronic structure or create new energy and charge transfer routes to enhance the optical, electrical, and structural stability of all-inorganic lead halide perovskites. By the interaction of excitons and dopants, doping can bring additional optical, electronic, and magnetic features in addition to increasing the photocatalytic efficiency.[171,172]

3.2 Heterojunction construction

The formation of a heterojunction at the interface between two distinct materials can efficiently improve the separation efficiency of photogenerated carriers, thus enhancing the photocatalytic performance. There are three types of heterojunctions suitable for photocatalysis: type II heterojunction, direct Z-type heterojunction, and S-type heterojunction. Different types of heterojunctions and their applications are summarized in Table 5.

3.2.1 Type-II heterogeneous junction. As exhibited in Fig. 5a, type II heterojunction consists of two semiconductors with two energy levels interlocked. When exposed to light, photogenerated holes will be transfer from the semiconductor with lower valence band to the other semiconductor with higher valence band; meanwhile, photogenerated electrons will be excited from the semiconductor with higher conduction band to other semiconductor with lower conduction band for reduction, promoting the spatial separation of charge carriers.[197] Interestingly, the system of type-II heterojunctions not only enhances the photocatalytic ability but also improves the stability of all-inorganic lead-halide perovskites. Wang *et al.* developed a layer-by-layer $NiO_x/CsPbBr_3/TiO_2$ planar II heterojunction photocatalyst; the system demonstrated a 7-fold increase in photoactivity compared to $CsPbBr_3$.[198] Kamat *et al.* reported a quasi-type II $CsPbBr_3$–CdS core–shell heterojunction with significantly improved stability and photocatalytic performance.[178] Yin *et al.* reported an efficient $CsPbBr_3$/CdSe heterojunction photocatalytically to reduce CO_2 employing water as an electron donor in organic solutions.[199] The type II heterojunction with strong electronic coupling of the Pb–Se and Br–Cd bonds between CdSe and $CsPbBr_3$ facilitated the transfer of electrons, and the CO yield of the main product reached 115.26 $\mu mol\ g^{-1}$, which was 4.6 times higher than that of $CsPbBr_3$.

However, the type II heterojunction still has some issues: on the one hand, the oxidizing capacity of two semiconductor photocatalysts decreased by the separation of photogenerated electron–holes; on the other hand, the presence of holes prevents the transfer of electron–holes between surfaces in other catalysts.

3.2.2 Z-type heterogeneous junction. Z-type heterojunction also consists of two semiconductors with an alternating band arrangement (Fig. 5b). Under photoexcitation, the photogenerated holes of the semiconductor with the higher valence band will recombine with the photogenerated electrons from the semiconductor with the lower conduction band. The Z-type heterojunction structure can maintain the photocatalyst in the proper valence band position and can spatially separate electron–hole pairs to enhance redox capability.[195] Jiang *et al.* created an all-solid Z-type heterojunction by connecting $CsPbBr_3$ with -Fe_2O_3, and this Z-type photocatalyst[200] demonstrated a six-fold improvement in photocatalytic activity to convert CO_2 into fuel (CO and CH_4). Xue *et al.* fabricated a water-stable Z-type Ag/CsPbBr3/Bi_2WO_6 photocatalyst for the degradation of rhodamine B, and the catalyst degraded rhodamine B at a rate of 93.9% in 120 minutes, which was 4.41 times faster than Bi_2WO_6.[195]

It should be noted that unanticipated side effects will result from Z-type heterojunction. The Z-type heterojunction increases the electron and hole-driving force of photogenerated chemical reactions; however, half of the electrons and holes produced during the photosynthesis process are lost. Therefore, when designing and building all-inorganic lead-halide perovskite-based heterojunction photocatalysts, the reaction process and the necessary redox potential should be taken into account.

Table 5 Heterojunction type photocatalyst summary

No.	Photocatalyst	Type	Application	Reference
1	$WO_3/CsPbBr_3$	S	CO_2 reduction	173
2	C_3N_4@$CsPbBr_3$	Z	CO_2 reduction	174
3	$CsPbBr_3$–rGO/Bi_2WO_6	S	Norfloxacin degradation	175
4	α-Fe_2O_3/rGO/$CsPbBr_3$	Z	CO_2 reduction	176
5	$Cs_xWO_3/CsPbBr_3$	Z	Hydrogen generation	177
6	$CsPbBr_3$–CdS	II	Contaminant degradation	178
7	$CsPbBr_3$/GO	II	Photoconductivity	179
8	$CsPbBr_3/Bi_2WO_6$	Z	Pyrotechnic tar reduction	180
9	$Bi_2O_2Se/CsPbBr_3$	S	Light detection	181
10	$CsPb(Br/I)_3/SiO_2$	II	LED	90
11	$CsPbBr_3$/GeSn	II	Photodetector	182
12	$CsPbBr_3/TiO_2$	S	CO_2 reduction	183–186
13	$CsPbBr_3$/PbS	Z	Light detection	187
14	$CsPbBr_3/CsPb_2Br_5$	Z	LED	188
15	$CsPbBrCl_2$/g-C_3N_4	II	Photodegradable dyes	189 and 190
16	$CsPbBr_3$/GO–Pt	Z	Hydrogen generation	191
17	$CsPbBr_3/Cs_4PbBr_6$@COF	Z	Water spilt	192
18	$CsPbBr_3$–CdZnS	S	CO_2 reduction	121
19	$CsPbBr_3$/UiO-66	Z	Methyl orange degradation	193
20	$CsPbBr_3$@SnO_2	S	CO_2 reduction	194
21	Ag/$CsPbBr_3/Bi_2WO_6$	Z	Rhodamine B degradation	195
22	PCN-222/$CsPbBr_3$	Z	CO_2 reduction	196

3.2.3 S-type heterogeneous junction. As exhibited in Fig. 5c, the S-type heterojunction is formed by the interlaced structure of the reduced semiconductor photocatalyst with a low work function and high Fermi level as well as the oxidized semiconductor photocatalyst with a high work function and low Fermi level.[201] The S-type heterojunction achieves the spatial

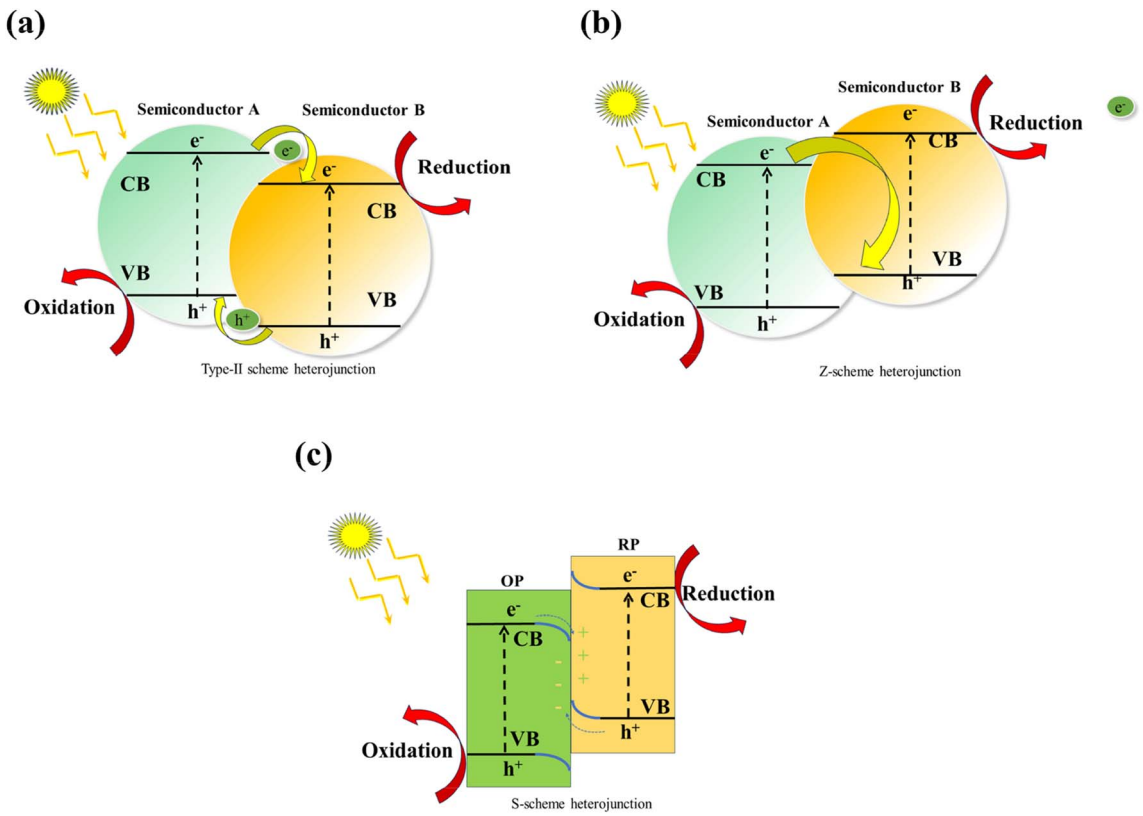

Fig. 5 Mechanism diagram of type-II heterojunction (a); mechanism diagram of Z-scheme heterojunction (b); mechanism diagram of S-scheme heterojunction (c).

separation of photogenerated electron–holes in the semiconductor with stable redox ability through the three methods of built-in electric field, energy band bending, and electrostatic contact.[202,203] Zhang *et al.* created $CsPbBr_3$ quantum dot/BiOBr nanosheets to reduce CO_2 with an electron consumption rate of 72.3 mol g^{-1} h^{-1}, which was 4.1 and 5.7 times higher than that of single $CsPbBr_3$ and BiOBr, respectively.[204] Xu *et al.* also created TiO_2/$CsPbBr_3$ S-type heterojunctions, which exhibited higher CO_2 reduction rates.[205] Pu *et al.* prepared $CsPbBr_3$/α-Fe_2O_3 S-type heterojunction,[206] and the electron consumption rate was 3.38 mmol g^{-1} h^{-1}, which was 2.4 times of that of the original $CsPbBr_3$.

In conclusion, all-inorganic halide perovskites are highly advantageous for photocatalysis due to their high absorption coefficient, defect tolerance, and variable band position. An extensive density of active sites, strong stability, and recyclability are also necessary for photocatalysts in addition to effective charge separation and transfer. In general, it is difficult for single-component halide perovskite photocatalysts to meet all these requirements. Integrating heterostructures of different functional materials into a single system through precise design is a common strategy to improve semiconductor performance because interactions between different components create synergistic effects. Consequently, halide-based perovskite heterostructures exhibit higher photocatalytic performance.

3.3 Other modification methods

3.3.1 Anion exchange method. By altering the X element in $CsPbX_3$, the anion exchange method could enhance the photocatalytic performance. Nedelcu *et al.* carried out anion exchange on $CsPbX_3$ (Cl, Br, I);[120] the results showed that this exchange can easily tune the emission color over the entire visible range. Guo *et al.* reported the use of mixed halide chalcogenides $CsPb(Br_x/Cl_{1-x})_3$ (x = 0.7, 0.5, 0.3) to reduce CO_2, which proceeded for 9 h under simulated sunlight with great stability and selectivity for the conversion of CO_2 to CO and CH_4.[207] Zhao *et al.* successfully oxidized toluene using an anion-exchange synthesis of $CsPbBr_xCl_{3-x}$/TiO_2 composite catalyst.[208] Faceting and morphological adjustment can also improve the photocatalytic activity of all-inorganic lead halide perovskites. Das *et al.* prepared $CsPbBr_3$ nanocrystals by adjusting the (110) and (200) facets and found that $CsPbBr_3$ exhibits shape-dependent optoelectronic properties.[209]

3.3.2 Ligand modification. The surface modification of all-inorganic lead halide compounds,[210,211] such as ligand modification,[212–214] can also increase their stability and photocatalytic performance. Surface ligands play a key role in forming perovskites, which not only affect the nucleation and growth processes but are also extremely important for charge transport and structural stability.[215–217]

3.3.3 Encapsulation. The resistance of all-inorganic lead halide perovskites to moisture, oxygen, light, and high temperatures is still a significant challenge because of their intrinsic ionic characteristics, which restricts their further development and practical applications.[218,219] Efforts have been made to encapsulate it in various materials over the years. It has been demonstrated that encapsulation with inert materials is a practical and efficient technique to avoid decomposition and increase stability against treatment conditions involving light, heat, and water.[220] Silica, organic polymers, metal oxides, and metal salts are some examples of the various protective materials that have been proposed.[221] It turns out that enhancing the thermal and photostability of mesoporous SiO_2 by incorporating perovskite nanocrystals is a wise decision. Liang *et al.* evaluated the difference in the optical stability before and after encapsulating $CsPbBr_3$ in nano-SiO_2.[222] These findings indicate that the SiO_2 shell can significantly increase the photothermal stability of the shell by successfully restraining anion exchange and photodegradation.

In addition to ion doping and heterostructure, other modification methods such as anion exchange, surface ligand modification, and encapsulation can improve the stability of all-inorganic lead halide perovskites while maintaining high photocatalytic activity. All-inorganic lead halide perovskites typically consist of an all-inorganic core capped with organic ligands. We hope to find the most suitable ligands for surface passivation that will bring out the best and unique properties of the perovskite, thus broadening its applicability. Furthermore, encapsulation with materials has been proven to be a feasible and effective way to prevent decomposition and improve stability to survive water, light, and heat treatment conditions.

The two problems of low photocatalytic efficiency and poor stability of all-inorganic lead halide perovskites and the proposed solutions were already mainly discussed. As mentioned above, (1) adding dopants to the photocatalytic system can increase the active sites of the photocatalyst to promote adsorption capacity and redox reactions. By introducing appropriate doping metal ions, especially transition metal ions, the E_g of the catalyst can be adjusted, and the recombination of electrons and holes can be suppressed; (2) the construction of heterojunction nanocomposites is considered as an alternative strategy to promote all-inorganic lead halide perovskite photocatalysts. Coupling different types of cocatalysts with all-inorganic lead halide perovskites can induce the separation of photogenerated carriers and maximize the photocatalytic efficiency; (3) the instability problem of all-inorganic lead halide perovskites could be solved. The top priority is to build a protective layer or encapsulate ligands. The existence of a protective layer can isolate the perovskite from the external environment and prevent its interaction.

4 Applications of all-inorganic halide perovskites

Environmental protection and sustainable energy development are two major problems. Green, efficient storage, and renewable solar energy can be achieved using solar radiation to form chemical fuels, which are hydrogen and oxygen (from water splitting) or methane (from CO_2 reduction). The attractive optical properties of all-inorganic halide perovskites (*e.g.*, high absorption coefficient in the UV-visible region, tunable band gap, and high PLQY) make them suitable candidates for solar-

driven photocatalytic applications. This section will provide an overview of the current state of development for all-inorganic lead halide perovskites in photocatalytic pollutant degradation, CO_2 reduction, and H_2 evolution.

4.1 Photocatalytic hydrogen production

H_2, as an ideal clean energy source in the 21st century, is considered as an alternative to fossil fuels. Photocatalytic hydrolysis for hydrogen production has potential applications, in which the photocatalyst $CsPbX_3$ has been widely utilized.[223–225] The balance between photocatalytic activity and stability of $CsPbBr_3$ is achieved through the rational control of surface ligands. Wang *et al.* successfully achieved photocatalytic hydrogen evolution by synthesizing $CsPbBr_3$/Pt–TiO_2 composites.[226] Song *et al.* prepared the $CsPbBr_3$@polyaniline, which was stable even in an aqueous solution and had a photocatalytic hydrogen generation efficiency of 4.81 mmol (h^{-1} g^{-1}).[227] Xiang *et al.* utilized Zn^{2+}-doped $CsPbBr_3$ nanocrystals to directly reduce hydrogen atoms in water, which exhibited excellent photocatalytic activity and enhanced hydrogen production efficiency.[228] Sun *et al.* developed a new $CsPbBr_3$ nanocrystalline coupled NiFe-LDH photocatalyst for high-efficiency photocatalytic CO_2 reduction,[229] and the photocatalyst's optimum electron consumption rate was 39.58 mol g^{-1} h^{-1}, which was higher than that of pristine NiFe-LDH.

Low-polarity solvents can be utilized to produce stable reaction conditions for photocatalytic hydrogen production. Sun *et al.* produced 0.8 mol per g hydrogen during 8 hours of simulated solar irradiation using ethyl acetate.[230] In hydrogen halide (HX, X = Br, I) solutions, all-inorganic lead halide perovskites also show high photocatalytic hydrogen generation efficiency, for example, $CsPbBr_{3-x}I_x$/Pt exhibited excellent hydrogen production performance with 224 mol h^{-1} in saturated aqueous HBr solution.[231]

The attractive optical properties of all-inorganic halide perovskites (*e.g.*, high absorption coefficient in the UV-visible region, tunable E_g, and high PLQY) make them suitable candidates to produce hydrogen. Despite the exciting progress, the field is still in its infancy and there is still much room for development in designing targeted reaction systems, improving the stability and efficiency, and eliminating the toxicity of halide systems in converting solar into chemical energy.

4.2 Photocatalytic reduction of CO_2

CO_2 and other greenhouse gases have been rapidly accumulating in the atmosphere[232] due to mankind's overreliance on fossil fuels, leading to severe and permanent effects on the ecosystem.[233,234] China is supposed to reach a "carbon peak" by 2030,[235] indicating that greenhouse gas emissions play an important role in environmental issues,; thus, photocatalytic reduction of CO_2 is considered the most promising method.[236–239] Due to their outstanding qualities, such as affordability, simplicity of the synthesis method, visible light absorption, high CO_2 adsorption surface area, and adjustable structure, all-inorganic lead halide perovskites have been proved as effective catalysts.[240–246] The all-inorganic lead-halide perovskite materials generate electron–hole pairs by absorbing solar energy, and the generated electrons can reduce CO_2 to high value-added chemicals such as CO,[247] CH_4,[248] CH_3OH,[249] HCHO,[250] HCOOH,[196] and C_2H_4.[251]

Hou *et al.* accomplished CO_2 reduction with $CsPbBr_3$ quantum dots in ethyl acetate/H_2O solution with reduction product yields of 4.3, 1.5, and 0.1 mol g^{-1} h^{-1} for CO, CH_4, and H_2, respectively, where the CO_2 reduction selectivity was approximately 100%[230] (Fig. 6). Currently, the surface modification of $CsPbX_3$ or the creation of multi-component composites is the most cost-effective and promising solution to several issues with pure $CsPbX_3$ in the photocatalytic reduction of CO_2. Xu *et al.* fabricated $CsPbBr_3$/GO nanocomposites, which showed a CO_2 reduction rate of 23.7 mol h^{-1} g^{-1}.[176] Additionally, to increase the effectiveness of CO_2 reduction, all-inorganic lead halide perovskites combined with other substances could generate heterojunctions. Wang *et al.* created a 0D/2D heterojunction photocatalyst with $CsPbBr_3$/Bi_2WO_6 nanosheets for the photocatalytic reduction of CO_2; the yield was 503 mol g^{-1}, which was 9.5 times greater than that of a single $CsPbBr_3$.[252]

The humidity stability, CO_2 capture capacity, and charge separation efficiency were significantly increased when $CsPbBr_3$ nanocrystals combined with metal–organic frameworks (MOFs) for the photocatalytic reduction of CO_2.[253] The performance of perovskite nanocrystals can be significantly influenced by the special structure of MOFs. Wan *et al.* combined $CsPbBr_3$ and UiO-66(NH_2)[254] to create a composite photocatalyst with $CsPbBr_3$ QDs/UiO-66(NH_2) MOF structure, which was able to convert CO_2 to chemical fuel in a non-aqueous system. The

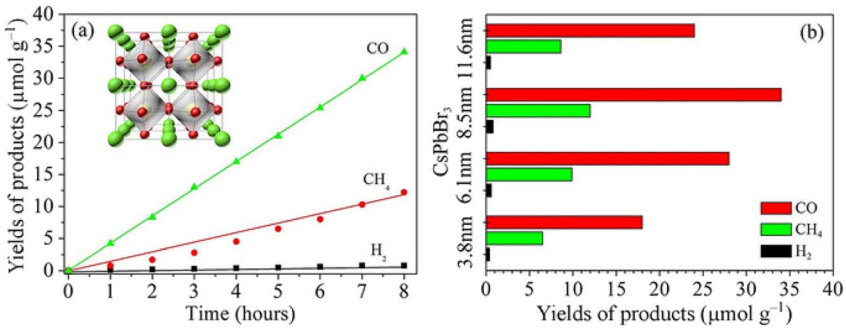

Fig. 6 Solar reduction CO_2 into fuels under 300 W Xe lamp irradiation by $CsPbBr_3$ quantum dots: 8.5 nm $CsPbBr_3$ quantum dots (a) and tunable $CsPbBr_3$ quantum dots with different particle sizes (b).[230]

Table 6 Reported all-inorganic lead halide perovskites photocatalytic reduction of CO_2

No.	Photocatalyst	Solution	Light source	Products and yield (μmol g^{-1} h^{-1})	Ref.
1	$CsPbBr_3$	Ethyl acetate/water	300 W xenon lamp	CO (4.25) CH_4 (1.5) H_2 (0.1)	230
2	$CsPbBr_3$–GO	Ethyl acetate	500 W xenon lamp	CH_4 (6.9)	255
3	$CsPbBr_3$/g-C_3N_4	Acetonitrile/water	300 W xenon lamp	CO (149)	256
4	$CsPbBr_3$/monolayered $Ti_3C_2T_x$	Ethyl acetate	300 W xenon lamp	CO (26.32) CH_4 (7.25)	257
5	$CsPbBr_3$/TiO_2	Ethyl acetate	300 W xenon lamp	H_2 (5.08) CO (7.73) CH_4 (10.12)	258
6	$CsPbBr_3$@zeolitic imidazolate	CO_2 and H_2O vapor	100 W xenon lamp	CO (0.67) CH_4 (3.33)	253
7	Fe–$CsPbBr_3$	Ethyl acetate/water	450 W xenon lamp	CO (3.2) CH_4 (6.1)	165

reported photocatalytic reduction of CO_2 by all-inorganic lead halide perovskites is summarized in Table 6.

All-inorganic lead halide perovskites are sensitive to water or other polar solvents, resulting in insufficient activity and low selectivity of all-inorganic lead halide perovskites. Therefore, it is considered a feasible method to improve the activity and stability of photocatalytic CO_2 reduction by means of element doping, morphology control, and construction of heterojunctions.

4.3 Contaminant degradation

Many harmful pollutants are emitted into the air, water, and soil as a result of the growth of the industry.[259–261] Photocatalysis is an effective method to degrade pollutants.[262–264] However, the efficiency of photocatalytic degradation of pollutants in water is still limited due to the low efficiency of solar energy utilization and the rapid recombination of photogenerated holes and electrons.[265–269] Among these materials for the photocatalytic degradation of pollutants, all-inorganic lead halide perovskite photocatalysts can efficiently utilize solar energy and have many advantages in terms of efficiency, greenness, and cost.[60] In particular, the photocatalytic degradation of organic dyes,[270–272] phenols,[273–275] and antibiotics[276–278] in water has generated a lot of interest in all-inorganic lead halide perovskites.

Among the various pollutants, synthetic dyes such as rhodamine B,[279–281] Sudan red III,[282–285] methyl red,[286–288] methyl violet,[289–293] malachite green,[294,295] acid black dye,[296–299] Congo red,[300] and methyl orange[301–303] are common. Feng *et al.* created $CsPb(Br_{1-x}Cl_x)_3$-Au nanoheterojunction materials,[271] which were used to decompose Sudan red III pollutants, and the results showed that after 6 hours of visible light exposure, the heterostructures had degraded 71% of Sudan dye. Liu *et al.* prepared $CsPbBr_3$ perovskite quantum dots/polymethyl methacrylate composites by ball milling; the degradation rate of rhodamine B by the composites under visible light reached 92.2% within 60 min.[304]

Besides dyes, the abuse of broad-spectrum antibiotics (ciprofloxacin,[305–307] norfloxacin,[308–311] 2-mercaptobenzothiazole,[312] and tetracycline hydrochloride[313–315]) causes harm to ecosystems and poses a threat to human health. Using all-inorganic lead halide perovskites, antibiotics can be successfully removed from water sources. Chen *et al.* produced all-inorganic $CsPbBr_3$ calcium titanite quantum dot materials by anti-solvent precipitation,[316] which was successfully used to remove antibiotic residues from ethanol, showing excellent photocatalytic activity. Zhao *et al.* synthesized Ag–$CsPbBr_3$/g-C_3N_4 ternary composites with excellent photocatalytic activity by loading nano-Ag on the surface of $CsPbBr_3$/bulky g-C_3N_4

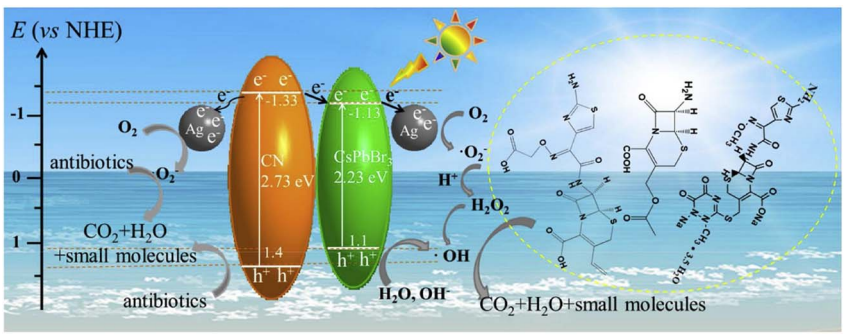

Fig. 7 Possible mechanism diagram for cephalosporin antibiotics degradation with Ag–$CsPbBr_3$/CN composite under visible light irradiation.[317]

Table 7 Summary of common all-inorganic lead-halide perovskites in terms of synthesis, modification, and application

Application	Sample	Synthesis method	Photocatalytic performance	Stability	Ref.
CO_2 reduction	$CsPb(Br_{0.5}/Cl_{0.5})_3$	Hot injection	Total yield of CO and CH_4 up to 875 μmol g^{-1} (99% selectivity) (ethyl acetate solution)	The PXRD patterns of $CsPb(Br_{0.5}/Cl_{0.5})_3$ did not change significantly after photocatalysis	207
	$CsPbBr_3$	Hot injection	CO evolution rate was 204.4 μmol g^{-1} h^{-1} and (100% selectivity)	Under 35 hours of irradiation, the production of CO increased with the extension of irradiation time	318
	$CsPbBr_3$@SnO_2	Solvothermal method and hot-injection	It showed a total production yield of 208.3 μmol g^{-1} (192.3 μmol g^{-1} for CO, and 16.0 μmol g^{-1} for CH_4) after 4 h	After four catalytic runs (4 h each). The result showed that no obvious decrease in activity was perceived for C_sPbBr_3@SnO_2	194
	$CsPbBr_3/MoS_2$	Ultrasonic method	CO yield of 74.9 μmol g^{-1} g^{-1} (ethyl acetate solution)	The conversion of CO_2 to CO and CH_4 decreased slightly by about 3.4% and 9.1%, respectively, after three cycles	319
	$CsPbI_3$/rGO	Hot injection	Formate generation with high selectivity (>90% $FE_{formate}$) ($KHCO_3$ solution)	Remaining stable in aqueous environments, rGO films provide significant protection for $CsPbI_3$ from the aqueous environment	320
	$CsPbBr_3$/alpha-Fe_2O_3	LARP	Showed electron consumption rate of 1.42 mmol g^{-1} h^{-1}	The activity can be maintained at 90% after three cycles	206
Wastewater degradation	$CsPbBr_3$	Emulsion and demulsion method	1 mg of catalyst can decompose an MO solution into a colorless solution in 100 min	The photocatalytic activity of $CsPbBr_3$ did not change significantly after two cycles	272
	Ti_3C_2-MXene/NiO/$CsPbI_3$	Hydrothermal	92.8% degradation of CV dye (15 mg L^{-1}) achieved in 90 min	After eight consecutive cycles of degradation, the photocatalytic degradation activity of CV dye slightly decreased by 2.9%	321
	$CsPbCl_3$	Facile solution-based technique	Degraded 90% of eosin-B dye in 180 min	Photocatalytic activity did not change after 3 cycles	322
	Co/$CsPbCl_3$	Solvothermal	Degraded 90% of MB dye in 180 min under visible light conditions	After three cycles of experiment, the degradation rate dropped by only 6%	323
	$CsPbCl_3$/CN	Hot injection	The degradation rate of 6-APA was 83.31% in 120 min	The photocatalytic activity did not change significantly after three cycles	276
	$CsPbBr_3$/MOF-808	Mechanochemical method	Cr(VI) reduction rate reached 92%; antibiotic degradation rate reached 97% (120 min)	After three runs, the PXRD patterns, FTIR spectra, and SEM image confirmed the stability of $CsPbBr_3$/MOF-808	324
	$CsPbI_3$/g-C_3N_4	Ultrasonic method	The degradation rate of RhB was 100% in 80 min (5 mg L^{-1})	After four cycles, the degradation efficiency was not reduced	325
	$CsPbI_3$	Hydrothermal method	The degradation rate of methyl violet was 81.7% in 120 min (5 mg L^{-1})	After three cycles, the degradation efficiency was slightly reduced	326
H_2 production	$CsPbBr_3$@ZIF-8	Ball milling	Exhibited an H_2 yield of 19.63 μmol g^{-1} after 2.5 h	Photoluminescence intensity remained around 86.7% after 8 weeks	58
	$CsPbBr_3$	Hot injection	Exhibited an H_2 evolution rate of 13.3 μmol g^{-1} h^{-1}	Photocatalytic activity did not change significantly after 20 h	57
	$CsPbBr_3$/GO–Pt	Anti-solvent precipitation method	Exhibited an H_2 evolution rate of 1060 μmol g^{-1} h^{-1} with high selectivity (>99%)	The photocatalyst showed no obvious deactivation with consistent H_2 after 20 h	191
	$CsPbBr_3$	Hot-injection	The amount of H_2 was 132 μmol g^{-1} within 4 h	H_2 generation with outstanding stability (≥160 h)	223
	Pt@δ-$CsPbI_3$	Solvothermal method	H_2 production reached 12.6 mmol g^{-1} h^{-1}	The activity of the material was constant within 24 h	327

composites[317] (Fig. 7), which were applied to the visible light catalytic degradation of 7-aminocephalosporanic acid; 7%-Ag–$CsPbBr_3$/g-C_3N_4 composites showed excellent photocatalytic activity, and 92.79% of 7-aminocephalosporanic acid was degraded. The stability and electron–hole separation rate of photocatalytic reactions can generally be improved by the heterostructures. Zhao *et al.* created type II $CsPbCl_3$ heterostructures,[276] and the catalysts showed excellent photocatalytic

performance for the degradation of penicillin–6-amino-penicillins acid. Liu *et al.* synthesized stable $CsPbBr_3$–TiO_2 heterojunction, which was applied in the visible light-driven photodegradation of tetracycline hydrochloride;[56] 80% of tetracycline hydrochloride was degraded in this experiment.

Oxygen activation typically initiates photodegradation reactions by generating reactive oxygen species (such as ·OH and $\cdot O^{2-}$), which react with the target pollutants. When all-inorganic lead halide perovskites are used as photocatalysts to breakdown organic dyes, some encouraging results have been obtained. All-inorganic lead halide perovskites have attracted great interest due to their excellent optoelectronic properties. Table 7 summarizes the application of all-inorganic lead halide perovskites in the field of photocatalysis, including CO_2 reduction, H_2 evolution, and degradation of pollutants in water. Inspired by natural photosynthesis, artificial photocatalysts that can convert solar energy into useable fuels and chemicals have been extensively studied. The structure of photocatalytic systems has been extensively studied to improve the photocatalytic activity; however, the problems of poor light absorption and conversion efficiency still need to be improved. Researchers are investigating possible strategies to improve the light harvesting and conversion efficiency of efficient photocatalysts. In addition to the effectiveness of the photocatalyst, the environmental friendliness, durability, and recyclability of the materials have also been focused on.

5 Challenges and prospects

All-inorganic lead halide perovskites have made significant progress in the field of photocatalysis. However, the strong ionic character of this substance makes its interior structure less stable. In addition, the existing reports have insufficient research on the growth kinetics of all-inorganic lead halide perovskite in the actual manufacturing process, which makes it difficult to control the formation and leads to low practical application efficiency, mainly due to the following aspects.

(1) The toxicity of lead is the main reason that restricts the actual production and large-scale commercial application of all-inorganic lead halide perovskites. Lead poisoning in humans can result in major health issues such as renal failure, nerve damage, and other disorders even at very low exposure levels.

(2) Due to the inherent ionic nature of all-inorganic lead halide perovskites, the resistance to moisture, oxygen, light, and high temperatures remains a significant challenge, and the perovskite structure is destroyed when exposed to polar solvents or water, which reduces its photocatalytic activity and limits practical application.

(3) The corresponding mechanism of photocatalysis has been extensively studied, but the precise redox pathway is still unknown.

(4) Inorganic lead halide perovskites have weak thermal and light stability and are easily harmed by external stimuli like heat, light, and oxygen.

Future enhancements will mostly focus on the following areas in response to the aforementioned issues.

(1) To reduce the toxicity of inorganic lead halide perovskites, it is necessary to develop efficient and environment-friendly lead-free metal halide perovskites by replacing Pb with other transition metals (such as Sn, Ge, Bi, and Ag). However, the activity of lead-free perovskites will be reduced. Therefore, the development of such lead-free photocatalysts should be combined with several improvement strategies.

(2) To simultaneously maintain high stability and catalytic activity, the A-site is modified with mixed ions. Mixing organic cations and inorganic cations to prepare organic–inorganic hybrid halide perovskites is a promising method. By this way, organic components can be added to improve the photocatalytic activity while retaining the stability of inorganic components. Common hybrid organic cations include FA^+ and MA^+; however, the ratio between organic and inorganic ions needs to be further refined.

(3) The development of novel protective layers or ligands to form a core–shell structure should be taken into consideration to address the deficiencies of inorganic perovskite's poor stability. Stable co-catalysts can be developed to form the same structure as various heterojunctions that match the energy bands of inorganic lead halide perovskites.

(4) Photocatalysis can be widely used in various fields. Exploring novel photocatalytic applications, such as (i) removal of organic matter and heavy metals in soil. Inorganic lead halide perovskite catalysts have strong redox capabilities and have broad application prospects in remediating soil organic matter and heavy metals. (ii) Organic synthesis: photocatalytic organic synthesis is an economical and green synthesis method that uses sunlight to drive chemical reactions under mild conditions. Many photoreduction reactions proceed *via* free radicals or radical ion intermediates. This reactive intermediate can be easily and efficiently generated by visible light. (iii) Environmental monitoring: with the continuous development of the chemical industry, the discharge of various pollutants has led to an increasing demand for the detection of various heavy metals and other pollutants present in waters. Utilizing the luminescent properties of all-inorganic lead halide perovskites is considered a highly sensitive detection method.

In summary, the development of catalysts with excellent catalytic properties is crucial for practical applications. However, how to improve the activity of the catalyst while maintaining the stability of the catalyst requires more research. The problems and challenges encountered so far will motivate researchers to develop more effective perovskite catalysts in the future.

Conflicts of interest

There are no conflicts to declare.

Acknowledgements

This work was supported by Fundamental Research Funds for the Central Universities (2572022BA09), Natural Science Foundation of Heilongjiang Province of China (LH2023D003).

References

1 L. Wang, S. Li, I. M. Ahmad, G. Zhang, Y. Sun, Y. Wang, C. Sun, C. Jiang, P. Cui and D. Li, *Sci. Total Environ.*, 2023, **887**, 164055.
2 S. Kuskaya, F. Bilgili, E. Mugaloglu, K. Khan, M. E. Hoque and N. Toguc, *Renewable Energy*, 2023, **206**, 858–871.
3 A. Wazeer, A. Das and S. Vidya, *Trans. Indian Inst. Met.*, 2023, **76**, 1155–1163.
4 J. Zheng and B. Zeng, *Sustain. Energy Technol. Assess.*, 2023, **57**, 103303.
5 A. Fujishima and K. Honda, *Nature*, 1972, **238**, 37–38.
6 J. Luo, Z. Wang, H. Jiang, S. Liu, F.-Q. Xiong and J. Ma, *Langmuir*, 2020, **36**, 4637–4644.
7 C. Xie, W. Chen, S. Du, D. Yan, Y. Zhang, J. Chen, B. Liu and S. Wang, *Nano Energy*, 2020, **71**, 104653.
8 T. Paik, M. Cargnello, T. R. Gordon, S. Zhang, H. Yun, J. D. Lee, H. Y. Woo, S. J. Oh, C. R. Kagan, P. Fornasiero and C. B. Murray, *ACS Energy Lett.*, 2018, **3**, 1904–1910.
9 L. Yin, X. Hai, K. Chang, F. Ichihara and J. Ye, *Small*, 2018, **14**, 1704153.
10 M. Shen, Z. Yan, L. Yang, P. Du, J. Zhang and B. Xiang, *Chem. Commun.*, 2014, **50**, 15447–15449.
11 L. Guo, C. Zhong, L. Shi, L. Ju, X. Wang, D. Yang, K. Bi, Y. Hao and Y. Yang, *Adv. Opt. Mater.*, 2019, 7, 1801403.
12 Y. Zou, J. W. Shi, D. Ma, Z. Fan, L. Cheng, D. Sun, Z. Wang and C. Niu, *ChemSusChem*, 2018, **11**, 1187–1197.
13 P. Kumar, S. Kataria, S. Roy, A. Jaiswal and V. Balakrishnan, *ChemistrySelect*, 2018, **3**, 7648–7655.
14 D. Zeng, L. Xiao, W. J. Ong, P. Wu, H. Zheng, Y. Chen and D. L. Peng, *ChemSusChem*, 2017, **10**, 4624–4631.
15 F. He, Z. Wang, Y. Li, S. Peng and B. Liu, *Appl. Catal., B*, 2020, **269**, 118828.
16 C. Xu, P. Ravi Anusuyadevi, C. Aymonier, R. Luque and S. Marre, *Chem. Soc. Rev.*, 2019, **48**, 3868–3902.
17 E. E. Barton, D. M. Rampulla and A. B. Bocarsly, *J. Am. Chem. Soc.*, 2008, **130**, 6342–6344.
18 T. Arai, S. Sato, T. Kajino and T. Morikawa, *Energy Environ. Sci.*, 2013, **6**, 1274–1282.
19 Y. Chen, B. Jia, G. Qin, H. Zhao, L. Han and P. Lu, *RSC Adv.*, 2023, **13**, 15055–15062.
20 A. Dabbous, E. Colson, D. Chakravorty, J.-M. Mouesca, C. Lombard, S. Caillat, J.-L. Ravanat, F. Dubois, F. Denes, P. Renaud and V. Maurel, *Chem.–Eur. J.*, 2023, **29**, e202300303.
21 M. Asim, S. Zhang, B. Maryam, J. Xiao, C. Shi, L. Pan and J.-J. Zou, *Appl. Surf. Sci.*, 2023, **620**, 156787.
22 X. Li, J. Hu, Y. Deng, T. Li, Z.-Q. Liu and Z. Wang, *Appl. Catal., B*, 2023, **324**, 122243.
23 F. Wang, J. Li, X. Yu, H. Tang, J. Xu, L. Sun and Q. Liu, *J. Mater. Sci. Technol.*, 2023, **146**, 49–60.
24 X. Feng and L. Zhang, *J. Mater. Sci. Technol.*, 2023, **156**, 54–63.
25 A. U. Hasanah, P. L. Gareso, N. Rauf and D. Tahir, *ChemBioEng Rev.*, 2023, **10**, 698–710.
26 A. Sinha, S. K. Sahu, S. Biswas and T. K. Ghorai, *RSC Adv.*, 2023, **13**, 22029–22042.
27 Y. Xue, Y. Guo, Z. Liang, H. Cui and J. Tian, *J. Colloid Interface Sci.*, 2019, **556**, 206–213.
28 C. Lu, E. Wu, C. Li, W. Dou, Y. Lian, Y. Liang, X. Xiang and H. Wang, *J. Phys. Chem. Solids*, 2021, **158**, 110228.
29 R. Ranjan, M. Kumar and A. S. K. Sinha, *Int. J. Hydrogen Energy*, 2019, **44**, 16176–16189.
30 N. Sharma, S. Swami, V. Shrivastava, R. Nair and R. Shrivastava, *Mater. Today: Proc.*, 2021, **43**, 3309–3317.
31 F. Cai, J. J. Ibrahim, Y. Fu, W. Kong, J. Zhang and Y. Sun, *Appl. Catal., B*, 2020, **264**, 118500.
32 L. Gui, Y. Xu, Q. Tang, X. Shi, J. Zhang, B. He and L. Zhao, *J. Colloid Interface Sci.*, 2021, **603**, 252–258.
33 X. Wang, Z. Zhu, J. Jiang, R. Li and J. Xiong, *Chemosphere*, 2023, **337**, 139206.
34 T. Xu, R. Wang, C. Gu and T. Jiang, *Spectrochim. Acta, Part A*, 2023, **299**, 122801.
35 W. Ashraf, S. H. Parvez and M. Khanuja, *Environ. Res.*, 2023, **236**, 116715.
36 L. Li, H. Yang and P. Yang, *J. Colloid Interface Sci.*, 2023, **650**, 1312–1318.
37 S. Liu, X. Zhou, J. Qin, C. Wei and Y. Hu, *J. Colloid Interface Sci.*, 2023, **635**, 59–71.
38 Q. Ding, X. Zou, J. Ke, Y. Dong, Y. Cui and H. Ma, *J. Colloid Interface Sci.*, 2023, **649**, 148–158.
39 Z. Jiang, Q. Long, B. Cheng, R. He and L. Wang, *J. Mater. Sci. Technol.*, 2023, **162**, 1–10.
40 R. Del Sole, C. Lo Porto, S. Lotito, C. Ingrosso, R. Comparelli, M. L. Curri, G. Barucca, F. Fracassi, F. Palumbo and A. Milella, *Molecules*, 2023, **28**, 5131.
41 A. Saleem, F. F. Alharbi, M. N. Ashiq, S. Manzoor, S. I. Abbas Shah, K. Z. Khan, S. Aman, N. Ahmad, H. A. Alzahrani and M. Messali, *Phys. Status Solidi A*, 2023, **220**, 2200734.
42 Y. Yang, Y. Sun and Y. Jiang, *Mater. Chem. Phys.*, 2006, **96**, 234–239.
43 P. Priyadarshini, S. Das and R. Naik, *RSC Adv.*, 2022, **12**, 9599–9620.
44 X. Zhu, Y. Lin, J. San Martin, Y. Sun, D. Zhu and Y. Yan, *Nat. Commun.*, 2019, **10**, 2843.
45 P. Priyadarshini, S. Senapati and R. Naik, *Renewable Sustainable Energy Rev.*, 2023, **186**, 113649.
46 J. M. Frost, K. T. Butler, F. Brivio, C. H. Hendon, M. van Schilfgaarde and A. Walsh, *Nano Lett.*, 2014, **14**, 2584–2590.
47 A. Walsh, *J. Phys. Chem. C*, 2015, **119**, 5755–5760.
48 S. R. Mulani, S. Bimli, E. Choudhary, R. Bunkar, U. A. Kshirsagar and R. S. Devan, *Chemosphere*, 2023, **340**, 139890.
49 D. Komaraiah, E. Radha, J. Sivakumar, M. V. Ramana Reddy and R. Sayanna, *Opt. Mater.*, 2020, **108**, 110401.
50 Q. Zhang, X. Deng, C. Tan, Y. Zhou, X. Chen, X. Bai, J. Li, B. Tang, S. Li and H. Lin, *J. Chem. Phys.*, 2020, **153**, 024703.
51 Z. Lu, J. Gao, S. Rao, C. Jin, H. Jiang, J. Shen, X. Yu, W. Wang, L. Wang, J. Yang and Q. Liu, *Appl. Catal., B*, 2024, **342**, 123374.

52 Q. Guo, J.-D. Zhang, Y.-J. Chen, K.-Y. Zhang, L.-N. Guo, Q.-C. Shan, J.-L. Lu, X.-H. Duan and L.-Z. Wu, *Chem. Commun.*, 2023, **59**, 4189–4192.
53 A. Sabbah, I. Shown, M. Qorbani, F.-Y. Fu, T.-Y. Lin, H.-L. Wu, P.-W. Chung, C.-I. Wu, S. R. M. Santiago, J.-L. Shen, K.-H. Chen and L.-C. Chen, *Nano Energy*, 2022, **93**, 106809.
54 K. Su, S.-X. Yuan, L.-Y. Wu, Z.-L. Liu, M. Zhang and T.-B. Lu, *Small*, 2023, **19**, 2301192.
55 H. Peng, L. Duan, W. Xie, C. Shao, H. Cao, D. Wang, S. Rao and H. Guo, *Chemosphere*, 2024, **346**, 140614.
56 C. Liu, X. Qian, Q. Wei, Z. Chen, J. Chen, W. Wang, X. Chen, J. Gao, Y. Liu and L. Xie, *J. Cleaner Prod.*, 2022, **365**, 132830.
57 R.-J. Huang, Z.-K. Qin, L.-L. Shen, G. Lv, F. Tao, J. Wang and Y.-J. Gao, *J. Mater. Chem. A*, 2023, **11**, 6217–6225.
58 S. Feng, S. Ning, L. Wang, J. Zhao, J. Ou, Z. Wu, S. Luo, Z. Lin, K. Yan, C. Wu and Y. Xu, *ACS Appl. Energy Mater.*, 2022, **5**, 6248–6255.
59 N. Luo, C. Chen, D. Yang, W. Hu and F. Dong, *Appl. Catal., B*, 2021, **299**, 120664.
60 S. Gull, S. Batool, G. Li and M. Idrees, *Front. Chem.*, 2022, **10**, 1020484.
61 D. Wang, C. Miao, H. Li, B. Yu, W. Wang, Y. Wang, G. Che, C. Liu and B. Hu, *Mater. Res. Bull.*, 2024, **170**, 112552.
62 W. Liu, H. Xie, X. Guo, K. Wang, C. Yang, N. Wang and C. Ge, *Opt. Mater.*, 2023, **136**, 113398.
63 J. Cui, C. Xu, Z. Jin, H. Liu, R. Hu and F. Liu, *Environ. Sci. Pollut. Res.*, 2023, **30**, 96875–96890.
64 H. Mohan, S. Vadivel and T. Shin, *Ultrason. Sonochem.*, 2023, **101**, 106650.
65 H. Zhang, F. Meng, H. Wei, W. Yu and S. Yao, *J. Colloid Interface Sci.*, 2023, **652**, 1282–1296.
66 T. Ishii, A. Anzai, A. Yamamoto and H. Yoshida, *Appl. Catal., B*, 2020, **277**, 119192.
67 Q. Li, X. Bai, J. Luo, C. Li, Z. Wang, W. Wu, Y. Liang and Z. Zhao, *Nanotechnology*, 2020, **31**, 375402.
68 K. Sathiyamoorthy, A. Silambarasan, M. Navaneethan and S. Harish, *Chemosphere*, 2024, **348**, 140575.
69 D. E. Mazouzi, F. Djani, A. Soukeur, W. Bouchal, A. Manseri, K. Derkaoui, A. Martínez-Arias, A. Ksouri, F. Şen and M. M. Kaci, *Surf. Interfaces*, 2024, **44**, 103581.
70 G. E. de la Huerta-Hernández, J. Chávez-Carvayar, T. Rodríguez-Flores, I. Castro-Cisneros, A. Reyes-Montero and I. Hernández-Pérez, *Environ. Sci. Pollut. Res.*, 2023, **30**, 102986–103000.
71 V. K. Amritha and S. Badhulika, *New J. Chem.*, 2023, **47**, 17897–17907.
72 A. H. Jawhari, N. Hasan, I. A. Radini, K. Narasimharao and M. A. Malik, *Nanomaterials*, 2022, **12**, 2985.
73 A. S. Rodrigues, J. E. Silveira, J. Carbajo, J. A. Zazo, J. A. Casas, A. Fernandes, M. J. Pacheco, L. Ciriaco and A. Lopes, *Environ. Sci. Pollut. Res.*, 2021, **28**, 23822–23832.
74 Y. Zhang, W. Wang, Y. Guo, Q. Shen and Z. Liu, *J. Phys. Chem. Solids*, 2021, **149**, 109766.
75 X. Chen, Q. Dong, S. Chen, Z. Zhang, X. Zhang, Y. Di, A. Jiang, D. Zhang and T. Li, *Colloids Surf., A*, 2023, **664**, 131143.
76 F. Li, Z. Wu, X. Tang, X. Li, X. Liu, S. Yu, L. Wei and C. Yu, *J. Water Process. Eng.*, 2023, **56**, 104470.
77 S. Park, W. J. Chang, C. W. Lee, S. Park, H.-Y. Ahn and K. T. Nam, *Nat. Energy*, 2016, **2**, 16185.
78 W. Ma, T. Jiang, Z. Yang, H. Zhang, Y. Su, Z. Chen, X. Chen, Y. Ma, W. Zhu, X. Yu, H. Zhu, J. Qiu, X. Liu, X. Xu and Y. Yang, *Advanced Science*, 2021, **8**, 2003728.
79 F. Cao, D. Yu, W. Ma, X. Xu, B. Cai, Y. M. Yang, S. Liu, L. He, Y. Ke, S. Lan, K.-L. Choy and H. Zeng, *ACS Nano*, 2020, **14**, 5183–5193.
80 J. H. Heo, D. H. Shin, J. K. Park, D. H. Kim, S. J. Lee and S. H. Im, *Adv. Mater.*, 2018, **30**, 1801743.
81 L. Wang, K. Fu, R. Sun, H. Lian, X. Hu and Y. Zhang, *Nano-Micro Lett.*, 2019, **11**, 52.
82 Y. Zhou, J. Chen, O. Bakr and O. Mohammed, *ACS Energy Lett.*, 2021, **6**, 739–768.
83 X. Li, W. Cai, H. Guan, S. Zhao, S. Cao, C. Chen, M. Liu and Z. Zang, *Chem. Eng. J.*, 2021, **419**, 129551.
84 Y. Huang, L. Zhang, J. Wang, B. Zhang, L. Xin, S. Niu, Y. Zhao, M. Xu, X. Chu, D. Zhang, C. Qu and F. Zhao, *Opt. Lett.*, 2019, **44**, 1908–1911.
85 Q. Mo, C. Chen, W. Cai, S. Zhao, D. Yan and Z. Zang, *Laser Photonics Rev.*, 2021, **15**, 2100278.
86 M. Liu, M. B. Johnston and H. J. Snaith, *Nature*, 2013, **501**, 395–398.
87 Y. Zhou, Q. Gu, Y. Li, L. Tao, H. Tan, K. Yin, J. Zhou and S. Guo, *Nano Lett.*, 2021, **21**, 4861–4867.
88 Y. Zhao, J. Zhu, B. He and Q. Tang, *Chem. Commun.*, 2021, **57**, 7577–7580.
89 C. Ponti, G. Nasti, D. Di Girolamo, I. Cantone, F. A. Alharthi and A. Abate, *Trends Ecol. Evol.*, 2022, **37**, 281–283.
90 C. Sun, Y. Zhang, C. Ruan, C. Yin, X. Wang, Y. Wang and W. W. Yu, *Adv. Mater.*, 2016, **28**, 10088–10094.
91 H. C. Yoon, H. Kang, S. Lee, J. H. Oh, H. Yang and Y. R. Do, *ACS Appl. Mater. Interfaces*, 2016, **8**, 18189–18200.
92 G. Jin, T. Liu, Y. Li, J. Zhou, D. Zhang, P. Pang, Z. Ye, Z. Xing, G. Xing, J. Chen and D. Ma, *Nanoscale*, 2022, **14**, 919–929.
93 G. Xing, N. Mathews, S. S. Lim, N. Yantara, X. Liu, D. Sabba, M. Grätzel, S. Mhaisalkar and T. C. Sum, *Nat. Mater.*, 2014, **13**, 476–480.
94 S. Chen, K. Roh, J. Lee, W. K. Chong, Y. Lu, N. Mathews, T. C. Sum and A. Nurmikko, *ACS Nano*, 2016, **10**, 3959–3967.
95 L. Dou, Y. M. Yang, J. You, Z. Hong, W. H. Chang, G. Li and Y. Yang, *Nat. Commun.*, 2014, **5**, 5404.
96 J. Ding, S. Du, Z. Zuo, Y. Zhao, H. Cui and X. Zhan, *J. Phys. Chem. C*, 2017, **121**, 4917–4923.
97 W. Zhai, J. Lin, C. Li, S. Hu, Y. Huang, C. Yu, Z. Wen, Z. Liu, Y. Fang and C. Tang, *Nanoscale*, 2018, **10**, 21451–21458.
98 A. Bhardwaj, K. Kundu, R. Sasmal, P. Acharyya, J. Pradhan, S. Kalita, S. S. Agasti and K. Biswas, *Chem. Sci.*, 2023, **14**, 7161–7169.
99 M. Wang, S. Wang, R. Chen, M. Zhu, Y. Liu, H. Ding, J. Ren, T. Xuan and H. Li, *Coatings*, 2023, **13**, 1062.
100 H. Wei, T. Si, F. Xu, W. Fan, T. Yang, B. Cao, F. Juan, J. Xu and Y. Wu, *Opt. Express*, 2023, **31**, 25298–25306.

101 Y. Chen, S. Lu, M. Nan, J. Xie, W. Shen, A. N. Aleshin, G. Cheng, S. Chen and W. Huang, *Adv. Opt. Mater.*, 2023, **11**, 2300473.
102 Y. Ma, F. Zheng, S. Li, Y. Liu, J. Ren, Y. Wu, Q. Sun and Y. Hao, *ACS Appl. Mater. Interfaces*, 2023, **15**, 34862–34873.
103 A. Pieniazek, F. Dybala, M. P. Polak, L. Przypis, A. P. Herman, J. Kopaczek and R. Kudrawiec, *J. Phys. Chem. Lett.*, 2023, **14**, 6470–6476.
104 J. Hou, Z. Wang, P. Chen, V. Chen, A. K. Cheetham and L. Wang, *Angew. Chem., Int. Ed. Engl.*, 2020, **59**, 19434–19449.
105 C. Zhang, W. Li and L. Li, *Angew. Chem., Int. Ed. Engl.*, 2021, **60**, 7488–7501.
106 J. Cai, K. Gu, Y. Zhu, J. Zhu, Y. Wang, J. Shen, A. Trinchi, C. Li and G. Wei, *Chem. Commun.*, 2018, **54**, 8064–8067.
107 Y. Tong, E. Bladt, M. F. Aygüler, A. Manzi, K. Z. Milowska, V. A. Hintermayr, P. Docampo, S. Bals, A. S. Urban, L. Polavarapu and J. Feldmann, *Angew. Chem., Int. Ed. Engl.*, 2016, **55**, 13887–13892.
108 J. Yan, Q. Wang, T. Wei, L. Jiang, M. Zhang, X. Jing and Z. Fan, *ACS Nano*, 2014, **8**, 4720–4729.
109 M. S. Sander, M. J. Côté, W. Gu, B. M. Kile and C. P. Tripp, *Adv. Mater.*, 2004, **16**, 2052–2057.
110 M. Fu, J. Zhou, Q. Xiao, B. Li, R. Zong, W. Chen and J. Zhang, *Adv. Mater.*, 2006, **18**, 1001–1004.
111 R. Wu, S. Gong, L. Wu, H. Yu, Q. Han and W. Wu, *Phys. Chem. Chem. Phys.*, 2022, **24**, 8303–8310.
112 L. Protesescu, S. Yakunin, O. Nazarenko, D. N. Dirin and M. V. Kovalenko, *ACS Appl. Nano Mater.*, 2018, **1**, 1300–1308.
113 M. Chen, Y. Zou, L. Wu, Q. Pan, D. Yang, H. Hu, Y. Tan, Q. Zhong, Y. Xu, H. Liu, B. Sun and Q. Zhang, *Adv. Funct. Mater.*, 2017, **27**, 1701121.
114 V. A. Hintermayr, A. F. Richter, F. Ehrat, M. Döblinger, W. Vanderlinden, J. A. Sichert, Y. Tong, L. Polavarapu, J. Feldmann and A. S. Urban, *Adv. Mater.*, 2016, **28**, 9478–9485.
115 L. Protesescu, S. Yakunin, M. I. Bodnarchuk, F. Krieg, R. Caputo, C. H. Hendon, R. X. Yang, A. Walsh and M. V. Kovalenko, *Nano Lett.*, 2015, **15**, 3692–3696.
116 A. A. M. Brown, P. Vashishtha, T. J. N. Hooper, Y. F. Ng, G. V. Nutan, Y. Fang, D. Giovanni, J. N. Tey, L. Jiang, B. Damodaran, T. C. Sum, S. H. Pu, S. G. Mhaisalkar and N. Mathews, *Chem. Mater.*, 2021, **33**, 2387–2397.
117 X. Li, Y. Wu, S. Zhang, B. Cai, Y. Gu, J. Song and H. Zeng, *Adv. Funct. Mater.*, 2016, **26**, 2435–2445.
118 X. l. Zeng, L. x. Yu, K. l. Peng, Y. Yu, Y. k. Deng, Y. j. Zhao and Y. n. Xu, *J. Alloys Compd.*, 2023, **945**, 169213.
119 Q. Pan, H. Hu, Y. Zou, M. Chen, L. Wu, D. Yang, X. Yuan, J. Fan, B. Sun and Q. Zhang, *J. Mater. Chem. C*, 2017, **5**, 10947–10954.
120 G. Nedelcu, L. Protesescu, S. Yakunin, M. I. Bodnarchuk, M. J. Grotevent and M. V. Kovalenko, *Nano Lett.*, 2015, **15**, 5635–5640.
121 Y. Wang, J. Wang, M. Zhang, S. Zheng, J. Wu, T. Zheng, G. Jiang and Z. Li, *Small*, 2023, **19**, e2300841.
122 A. Pan, B. He, X. Fan, Z. Liu, J. J. Urban, A. P. Alivisatos, L. He and Y. Liu, *ACS Nano*, 2016, **10**, 7943–7954.
123 J. Leng, T. Wang, Z. K. Tan, Y. J. Lee, C. C. Chang and K. Tamada, *ACS Omega*, 2022, **7**, 565–577.
124 Y. Yang, S. Wei, X. Kang, O. Tegus and D. Pan, *J. Lumin.*, 2019, **211**, 26–31.
125 C. M. Guvenc, A. Kocabas and S. Balci, *J. Mater. Chem. C*, 2023, **11**, 3039–3049.
126 S. Sun, D. Yuan, Y. Xu, A. Wang and Z. Deng, *ACS Nano*, 2016, **10**, 3648–3657.
127 X. Zhang, X. Bai, H. Wu, X. Zhang, C. Sun, Y. Zhang, W. Zhang, W. Zheng, W. W. Yu and A. L. Rogach, *Angew. Chem., Int. Ed. Engl.*, 2018, **57**, 3337–3342.
128 L. Rao, Y. Tang, C. Song, K. Xu, E. T. Vickers, S. Bonabi Naghadeh, X. Ding, Z. Li and J. Z. Zhang, *Chem. Mater.*, 2018, **31**, 365–375.
129 L. Rao, X. Du, G. Liang, Y. Tang, K. Tang and Z. Jin, *Beilstein J. Nanotechnol.*, 2019, **10**, 666–676.
130 Y. El Ajjouri, F. Palazon, M. Sessolo and H. Bolink, *Chem. Mater.*, 2018, **30**, 7423–7427.
131 G. Jiang, C. Guhrenz, A. Kirch, L. Sonntag, C. Bauer, X. Fan, J. Wang, S. Reineke, N. Gaponik and A. Eychmüller, *ACS Nano*, 2019, **13**, 10386–10396.
132 J. Kim, N. T. Manh, H. T. Thai, S. K. Jeong, Y. W. Lee, Y. Cho, W. Ahn, Y. Choi and N. Cho, *Nanomaterials*, 2022, **12**, 920.
133 Q. Zhang, W. Zheng, Q. Wan, M. Liu, X. Feng, L. Kong and L. Li, *Adv. Opt. Mater.*, 2021, **9**, 2002130.
134 Z. Long, S. Yang, J. Pi, D. Zhou, Q. Wang, Y. Yang, H. Wu and J. Qiu, *Ceram. Int.*, 2022, **48**, 35474–35479.
135 H. T. Ramolahloane, G. B. Nair and H. C. Swart, *Mater. Res. Bull.*, 2023, **165**, 112285.
136 X. Wu, K. Yin, M. Yang, Y. Hu and H. Peng, *Flexible Printed Electron.*, 2023, **8**, 035008.
137 S. Ye, M. Huang, Q. Han, J. Song and J. Qu, *J. Alloys Compd.*, 2023, **965**, 171442.
138 Y. Ji, L. Liang, T. Ma, J. Hu, Z. Chen and J. Chen, *Opt. Mater.*, 2023, **143**, 114254.
139 P. V. Kamat, *J. Phys. Chem. C*, 2007, **111**, 2834–2860.
140 J. Yang, D. Wang, H. Han and C. Li, *Acc. Chem. Res.*, 2013, **46**, 1900–1909.
141 J. Low, S. Cao, J. Yu and S. Wageh, *Chem. Commun.*, 2014, **50**, 10768–10777.
142 X. Li, J. Yu and M. Jaroniec, *Chem. Soc. Rev.*, 2016, **45**, 2603–2636.
143 R. Asahi, T. Morikawa, T. Ohwaki, K. Aoki and Y. Taga, *Science*, 2001, **293**, 269–271.
144 U. Diebold, *Surf. Sci. Rep.*, 2003, **48**, 53–229.
145 V. Subramanian, E. E. Wolf and P. V. Kamat, *J. Am. Chem. Soc.*, 2004, **126**, 4943–4950.
146 J. Low, J. Yu, Q. Li and B. Cheng, *Phys. Chem. Chem. Phys.*, 2014, **16**, 1111–1120.
147 M. S. Akple, J. Low, S. Wageh, A. A. Al-Ghamdi, J. Yu and J. Zhang, *Appl. Surf. Sci.*, 2015, **358**, 196–203.
148 Y. Bessekhouad, D. Robert and J. V. Weber, *J. Photochem. Photobiol., A*, 2004, **163**, 569–580.

149 N. Lamers, Z. Zhang, I. G. Scheblykin and J. Wallentin, *Adv. Opt. Mater.*, 2023, 2300435.
150 S. Wang, Z. Wei, L. Yu, J. Hou, G. Wu and Y. Xiao, *Chem. Eng. J.*, 2023, **468**, 143503.
151 L. Yu, Y. Wei, Y. Lei, C. Liu, Y. Liu and M. Hong, *CCS Chem.*, 2023, DOI: 10.31635/ccschem.023.202302845.
152 C. Zhang, M. Wang, J. Shi, J. Wang, Z. Da, Y. Zhou, Y. Xu, N. V. Gaponenko and A. S. Bhatti, *Front. Chem.*, 2023, **11**, 1199863.
153 D. J. Norris, N. Yao, F. T. Charnock and T. A. Kennedy, *Nano Lett.*, 2001, **1**, 3–7.
154 N. Pradhan and X. Peng, *J. Am. Chem. Soc.*, 2007, **129**, 3339–3347.
155 A. Malavika, S. Suresh, M. R. Subramaniam and S. K. Batabyal, *New J. Chem.*, 2023, **47**, 13783–13788.
156 Z. Wei, Y. Lv and X. Su, *Microchem. J.*, 2023, **192**, 108940.
157 A. Du, W. Zhao, Y. Peng, X. Qin, Z. Lin, Y. Ye, E. Chen, S. Xu and T. Guo, *Nanomaterials*, 2023, **13**, 17.
158 L. Jing, Q. Cen, Q. Pang and J. Z. Zhang, *J. Phys. Chem. C*, 2023, **127**, 2448–2455.
159 Y. Li, W. Li, Y. Yu and C. Zheng, *Opt. Mater. Express*, 2023, **13**, 1488–1496.
160 D. Patra and S. P. Singh, *J. Phys. Chem. C*, 2023, **127**, 9397–9406.
161 R. Yun, H. Yang, W. Sun, L. Zhang, X. Liu, X. Zhang and X. Li, *Laser Photonics Rev.*, 2023, **17**, 2200524.
162 R. Zhang, G. Chen, H. Liu, J. Zhang, Y. Yuan, Z. Lv, L. Zhang, C. Wang, Z. Qin, W. Yang and J. Wang, *Opt. Mater.*, 2023, **135**, 113308.
163 Y.-W. Liu, S.-H. Guo, S.-Q. You, C.-Y. Sun, X.-L. Wang, L. Zhao and Z.-M. Su, *Nanotechnology*, 2020, **31**, 215605.
164 J. V. Patil, S. S. Mali and C. K. Hong, *J. Energy Chem.*, 2021, **62**, 451–458.
165 S. Shyamal, S. K. Dutta and N. Pradhan, *J. Phys. Chem. Lett.*, 2019, **10**, 7965–7969.
166 G. X. Dong, W. Zhang, Y. F. Mu, K. Su, M. Zhang and T. B. Lu, *Chem. Commun.*, 2020, **56**, 4664–4667.
167 X. Zhou, Q. Chang, G. Xiang, S. Jiang, L. Li, X. Tang, F. Ling, Y. Wang, J. Li, Z. Wang and X. Zhang, *Spectrochim. Acta, Part A*, 2023, **300**, 122773.
168 W. Wang, S. Song, B. Cao and J. Li, *J. Lumin.*, 2022, **247**, 118901.
169 S. Huang, B. Wang, Q. Zhang, Z. Li, A.-d. Shan and L. Li, *Adv. Opt. Mater.*, 2018, **6**, 1701106.
170 E. Ouaaka, M. Aazza, A. Bouymajane and F. Cacciola, *Molecules*, 2023, **28**, 2880.
171 S. Paul, E. Bladt, A. F. Richter, M. Doeblinger, Y. Tong, H. Huang, A. Dey, S. Bals, T. Debnath, L. Polavarapu and J. Feldmann, *Angew. Chem., Int. Ed.*, 2020, **59**, 6794–6799.
172 N. Pradhan, *J. Phys. Chem. Lett.*, 2019, **10**, 2574–2577.
173 S. Jiang, Y. Song, H. Kang, B. Li, K. Yang, G. Xing, Y. Yu, S. Li, P. Zhao and T. Zhang, *ACS Appl. Mater. Interfaces*, 2022, **14**, 3385–3394.
174 H. Bian, D. Li, S. Wang, J. Yan and S. F. Liu, *Chem. Sci.*, 2022, **13**, 1335–1341.
175 Y. Zhao, X. Liang, X. Hu and J. Fan, *Colloids Surf., A*, 2021, **626**, 127098.
176 Y. F. Xu, M. Z. Yang, B. X. Chen, X. D. Wang, H. Y. Chen, D. B. Kuang and C. Y. Su, *J. Am. Chem. Soc.*, 2017, **139**, 5660–5663.
177 J.-Y. Li, H.-Y. Chen, Y. Jiang and D.-B. Kuang, *Sol. RRL*, 2021, **5**, 2100036.
178 A. Kipkorir, J. DuBose, J. Cho and P. Kamat, *Chem. Sci.*, 2021, **12**, 14815–14825.
179 H. Jin, Y. Chen, L. Zhang, R. Wan, Z. Zou, H. Li and Y. Gao, *Nanotechnology*, 2021, **32**, 085202.
180 R. Huang, M. Zhang, Z. Zheng, K. Wang, X. Liu, Q. Chen and D. Luo, *Nanomaterials*, 2021, **11**, 2422.
181 M. T. Hossain, M. Das, J. Ghosh, S. Ghosh and P. K. Giri, *Nanoscale*, 2021, **13**, 14945–14959.
182 H. Cong, X. Chu, F. Wan, Z. Chu, X. Wang, Y. Ma, J. Jiang, L. Shen, J. You and C. Xue, *Small Methods*, 2021, **5**, e2100517.
183 E. Zhu, Y. Zhao, Y. Dai, Q. Wang, Y. Dong, Q. Chen and Y. Li, *Chin. J. Chem.*, 2020, **38**, 1718–1722.
184 Y. Liu, Y. Yang, P. Chen, Y. Shan, Y. Li, J. Shi, J. Hou, N. Zhang, G. Zhao, J. Xu, Y. Fang and N. Dai, *Small*, 2020, **16**, e2004126.
185 Q. Huang, Z. Liang, F. Qi, N. Zhang, J. Yang, J. Liu, C. Tian, C. Fu, X. Tang, D. Wu, J. Wang, X. Wang and W. Chen, *J. Phys. Chem. Lett.*, 2022, **13**, 2418–2427.
186 X. Xiao, S. Guo, C. Ding, Z. Zhang, H. Huang and J. Xu, *J. Inorg. Mater.*, 2021, **36**, 507–512.
187 H. Zhao, Y. Zhang, T. Li, Q. Li, Y. Yu, Z. Chen, Y. Li and J. Yao, *Nanotechnology*, 2020, **31**, 035202.
188 Z. P. Huang, B. Ma, H. Wang, N. Li, R. T. Liu, Z. Q. Zhang, X. D. Zhang, J. H. Zhao, P. Z. Zheng, Q. Wang and H. L. Zhang, *J. Phys. Chem. Lett.*, 2020, **11**, 6007–6015.
189 T. Paul, D. Das, B. K. Das, S. Sarkar, S. Maiti and K. K. Chattopadhyay, *J. Hazard. Mater.*, 2019, **380**, 120855.
190 M. Shu, J. Lu, Z. Zhang, T. Shen and J. Xu, *J. Inorg. Mater.*, 2021, **36**, 1217.
191 T. Chen, M. Li, L. Shen, M. B. J. Roeffaers, B. Weng, H. Zhu, Z. Chen, D. Yu, X. Pan, M.-Q. Yang and Q. Qian, *Front. Chem.*, 2022, **10**, 833784.
192 P. Kour and S. P. Mukherjee, *J. Mater. Chem. A*, 2021, **9**, 6819–6826.
193 C. Zhang, J. Miao, L. Guo, T. Tan, W. Cai, X. Lei, Y. Li and Z. Wang, *Appl. Organomet. Chem.*, 2023, **37**, e7122.
194 Z. Dong, Y. Shi, Y. Jiang, C. Yao and Z. Zhang, *J. CO2 Util.*, 2023, **72**, 102480.
195 J.-R. Xue, R.-C. Xue, P.-Y. Chen, Y. Wang and L.-P. Yu, *J. Chin. Chem. Soc.*, 2023, **70**, 1481–1492.
196 P. Wang, X. Ba, X. Zhang, H. Gao, M. Han, Z. Zhao, X. Chen, L. Wang, X. Diao and G. Wang, *Chem. Eng. J.*, 2023, **457**, 141248.
197 H. McDaniel, P. E. Heil, C.-L. Tsai, K. Kim and M. Shim, *ACS Nano*, 2011, **5**, 7677–7683.
198 C. H. Wang, H. W. Huang, B. Weng, D. Verhaeghe, M. Keshavarz, H. D. Jin, B. Liu, H. P. Xie, Y. Ding, Y. J. Gao, H. F. Yuan, J. A. Steele, J. Hofkens and M. B. J. Roeffaers, *Appl. Catal., B*, 2022, **301**, 120760.
199 G. Yin, X. Qi, Y. Chen, Q. Peng, X. Jiang, Q. Wang, W. Zhang and X. Gong, *J. Mater. Chem. A*, 2022, **10**, 22468–22476.

200 Y. Jiang, J. F. Liao, H. Y. Chen, H. H. Zhang, J. Y. Li, X. D. Wang and D. B. Kuang, *Chem*, 2020, **6**, 766–780.
201 D.-E. Lee, N. Mameda, K. P. Reddy, B. M. Abraham, W.-K. Jo and S. Tonda, *J. Mater. Sci. Technol.*, 2023, **161**, 74–87.
202 J. Lu, S. Gu, H. Li, Y. Wang, M. Guo and G. Zhou, *J. Mater. Sci. Technol.*, 2023, **160**, 214–239.
203 M. Luo, G. Jiang, M. Yu, Y. Yan, Z. Qin, Y. Li and Q. Zhang, *J. Mater. Sci. Technol.*, 2023, **161**, 220–232.
204 Z. Zhang, L. Li, Y. Jiang and J. Xu, *Inorg. Chem.*, 2022, **61**, 3351–3360.
205 F. Xu, K. Meng, B. Cheng, S. Wang, J. Xu and J. Yu, *Nat. Commun.*, 2020, **11**, 4613.
206 Y.-C. Pu, Y.-H. Chuang, M.-W. Zheng, Y.-J. Chang and S.-H. Liu, *J. Environ. Chem. Eng.*, 2023, **11**, 109103.
207 S.-H. Guo, J. Zhou, X. Zhao, C.-Y. Sun, S.-Q. You, X.-L. Wang and Z.-M. Su, *J. Catal.*, 2019, **369**, 201–208.
208 Y. Zhao, Y. Dai, Q. Wang, Y. Dong, T. Song, A. Mudryi, Q. Chen and Y. Li, *ChemCatChem*, 2021, **13**, 2592–2598.
209 R. Das, A. Patra, S. K. Dutta, S. Shyamal and N. Pradhan, *J. Am. Chem. Soc.*, 2022, **144**, 18629–18641.
210 F.-B. Chiu, Y.-W. Wu and S.-H. Yang, *ACS Omega*, 2023, **8**, 19109–19118.
211 M. Giancaspro, R. Grisorio, G. Alò, N. Margiotta, A. Panniello, G. P. Suranna, N. Depalo, M. Striccoli, M. L. Curri and E. Fanizza, *Mater. Chem. Front.*, 2023, **7**, 2637–2650.
212 Y. Duan, K. Chordiya, M. U. Kahaly, F. E. Oropeza, V. A. de la Pena O'shea, D.-Y. Wang and R. D. Costa, *Adv. Opt. Mater.*, 2022, **10**, 2201176.
213 C. H. Tien, H.-H. Tsai and L. C. Chen, *J. Mater. Res. Technol.*, 2022, **19**, 3842–3851.
214 M. Wang, D. Liang, W. Ma, Q. Mo, Z. Zang, Q. Qian and W. Cai, *Opt. Lett.*, 2022, **47**, 4512–4515.
215 S. Bera, R. K. Behera, S. K. Dutta and N. Pradhan, *ACS Mater. Lett.*, 2023, **5**, 1332–1339.
216 M.-G. Jeon, A. Kirakosyan, C. Shin, S. Yun, J. Kim, L. Li and J. Choi, *Chem. Eng. J.*, 2023, **462**, 142120.
217 H. Wang, W. Lu, P. Xu, J. Luo, K. Yao, J. Zhang, X. Wei, S. Peng, H. Cheng, H. Hu and K. Sun, *ACS Sustainable Chem. Eng.*, 2023, **11**, 5963–5972.
218 Y. He, L. Zhang, G. Chen, Y. Liu, S. Shi, P. Jiang, J. Ding, S. Xu and C. Geng, *Appl. Surf. Sci.*, 2023, **611**, 155724.
219 C. Wang, M. Zhang, H. Yu, W. Zhang, G. Shi, X. Zhang, Z. Cui, P. Fu, M. Liu, X. Qiao, Y. He and X. Pang, *ACS Appl. Nano Mater.*, 2023, **6**, 3416–3424.
220 L. Wu, H. Hu, Y. Xu, S. Jiang, M. Chen, Q. Zhong, D. Yang, Q. Liu, Y. Zhao, B. Sun, Q. Zhang and Y. Yin, *Nano Lett.*, 2017, **17**, 5799–5804.
221 A. Pan, M. J. Jurow, F. Qiu, J. Yang, B. Ren, J. J. Urban, L. He and Y. Liu, *Nano Lett.*, 2017, **17**, 6759–6765.
222 X. Liang, W. Chen, J. Yang, X. Liu, X. Fang and W. Xiang, *ACS Appl. Electron. Mater.*, 2023, **5**, 2309–2317.
223 M. Xiao, M. Hao, M. Lyu, E. G. Moore, C. Zhang, B. Luo, J. Hou, J. Lipton-Duffin and L. Wang, *Adv. Funct. Mater.*, 2019, **29**, 19056831–19056838.
224 X. Zhang, M. He, H. Fang, J. Bao, X. Bu, C. Yang, X. Sheng, B. Wu, Z. Zhang and Y. Zhou, *Int. J. Hydrogen Energy*, 2022, **47**, 40860–40871.
225 M. Knezevic, V.-D. Quach, I. Lampre, M. Erard, P. Pernot, D. Berardan, C. Colbeau-Justin and M. N. Ghazzal, *J. Mater. Chem. A*, 2023, **11**, 6226–6236.
226 H. Wang, X. M. Wang, R. T. Chen, H. F. Zhang, X. L. Wang, J. H. Wang, J. Zhang, L. C. Mu, K. F. Wu, F. T. Fan, X. Zong and C. Li, *Int. J. Hydrogen Energy*, 2019, **4**, 40–47.
227 W. Song, Y. Wang, C. Wang, B. Wang, J. Feng, W. Luo, C. Wu, Y. Yao and Z. Zou, *ChemCatChem*, 2021, **13**, 1711–1716.
228 L. Ding, C. Shen, Y. Zhao, Y. Chen, L. Yuan, H. Yang, X. Liang, W. Xiang and L. Li, *Mol. Catal.*, 2020, **483**, 110764.
229 H. Sun, R. Tang, X. Zhang, S. Zhang, W. Yang, L. Wang, W. Liang, F. Li, R. Zheng and J. Huang, *Catal. Sci. Technol.*, 2023, **13**, 1154–1163.
230 J. Hou, S. Cao, Y. Wu, Z. Gao, F. Liang, Y. Sun, Z. Lin and L. Sun, *Chem.–Eur. J.*, 2017, **23**, 9481–9485.
231 Z. Guan, Y. Wu, P. Wang, Q. Zhang, Z. Wang, Z. Zheng, Y. Liu, Y. Dai, M.-H. Whangbo and B. Huang, *Appl. Catal., B*, 2019, **245**, 522–527.
232 N. S. Lewis and D. G. Nocera, *Proc. Natl. Acad. Sci. U. S. A.*, 2006, **103**, 15729–15735.
233 M. E. El-Khouly, E. El-Mohsnawy and S. Fukuzumi, *J. Photochem. Photobiol., C*, 2017, **31**, 36–83.
234 A. Crake, *Mater. Sci. Technol.*, 2017, **33**, 1737–1749.
235 W. Dong, Y. Ji, J. Wang, B. Li, F. Yang and J. Yang, *ACS Omega*, 2021, **6**, 34675–34686.
236 Y.-H. Chen, K.-A. Tsai, T.-W. Liu, Y.-J. Chang, Y.-C. Wei, M.-W. Zheng, S.-H. Liu, M.-Y. Liao, P.-Y. Sie, J.-H. Lin, S.-W. Tseng and Y.-C. Pu, *J. Phys. Chem. Lett.*, 2023, **14**, 122–131.
237 H. Xiao, Q. Qian and Z. Zang, *Sci. China Mater.*, 2023, **66**, 1810–1819.
238 Y.-J. Dong, Y. Jiang, J.-F. Liao, H.-Y. Chen, D.-B. Kuang and C.-Y. Su, *Sci. China Mater.*, 2022, **65**, 1550–1559.
239 D. Laishram, S. Zeng, K. M. Alam, A. P. Kalra, K. Cui, P. Kumar, R. K. Sharma and K. Shankar, *Appl. Surf. Sci.*, 2022, **592**, 153276.
240 C. Han, X. Zhu, J. S. Martin, Y. Lin, S. Spears and Y. Yan, *ChemSusChem*, 2020, **13**, 4005–4025.
241 J. Fan, B. Jia and M. Gu, *Photonics Res.*, 2014, **2**, 111–120.
242 S. A. Kulkarni, S. G. Mhaisalkar, N. Mathews and P. P. Boix, *Small Methods*, 2019, **3**, 1800231.
243 A. Tabish, A. M. Varghese, M. A. Wahab and G. N. Karanikolos, *Catalysts*, 2020, **10**, 95.
244 M. Singh and I. Sinha, *Sol. Energy*, 2020, **208**, 296–311.
245 S. Shyamal and N. Pradhan, *J. Phys. Chem. Lett.*, 2020, 6921–6934.
246 H. Huang, B. Pradhan, J. Hofkens, M. B. J. Roeffaers and J. A. Steele, *ACS Energy Lett.*, 2020, **5**, 1107–1123.
247 X. X. Chang, T. Wang and J. L. Gong, *Energy Environ. Sci.*, 2016, **9**, 2177–2196.
248 H.-L. Wu, X.-B. Li, C.-H. Tung and L.-Z. Wu, *Adv. Mater.*, 2019, **31**, 1900709.

249 W. Zhang, Z. Wang, P. Lin, D. Wu, Z. Shi, X. Chen, T. Xu, Y. Tian and X. Li, *J. Mater. Sci.*, 2020, **55**, 6826–6833.
250 G.-X. Dong, M.-R. Zhang, K. Su, Z.-L. Liu, M. Zhang and T.-B. Lu, *J. Mater. Chem. A*, 2023, **11**, 9989–9999.
251 X. Liu, J. Qiu, Q. Huang, X. Chen, J. Yu and J. Bao, *Phys. Chem. Chem. Phys.*, 2023, **25**, 11620–11629.
252 J. Wang, J. Wang, N. Li, X. Du, J. Ma, C. He and Z. Li, *ACS Appl. Mater. Interfaces*, 2020, **12**, 31477–31485.
253 Z.-C. Kong, J.-F. Liao, Y.-J. Dong, Y.-F. Xu, H.-Y. Chen, D.-B. Kuang and C.-Y. Su, *ACS Energy Lett.*, 2018, **3**, 2656–2662.
254 S. Wan, M. Ou, Q. Zhong and X. Wang, *Chem. Eng. J.*, 2019, **358**, 1287–1295.
255 Y.-H. Chen, J.-K. Ye, Y.-J. Chang, T.-W. Liu, Y.-H. Chuang, W.-R. Liu, S.-H. Liu and Y.-C. Pu, *Appl. Catal., B*, 2021, **284**, 119751.
256 M. Ou, W. Tu, S. Yin, W. Xing, S. Wu, H. Wang, S. Wan, Q. Zhong and R. Xu, *Angew. Chem., Int. Ed. Engl.*, 2018, **57**, 13570–13574.
257 A. Pan, X. Ma, S. Huang, Y. Wu, M. Jia, Y. Shi, Y. Liu, P. Wangyang, L. He and Y. Liu, *J. Phys. Chem. Lett.*, 2019, **10**, 6590–6597.
258 Y.-F. Xu, X.-D. Wang, J.-F. Liao, B.-X. Chen, H.-Y. Chen and D.-B. Kuang, *Adv. Mater. Interfaces*, 2018, **5**, 1801015.
259 O. Lefebvre and R. Moletta, *Water Res.*, 2006, **40**, 3671–3682.
260 J. Wang, J. Liu, Z. Du and Z. Li, *J. Energy Chem.*, 2021, **54**, 770–785.
261 D. Wang, S. C. Pillai, S.-H. Ho, J. Zeng, Y. Li and D. D. Dionysiou, *Appl. Catal., B*, 2018, **237**, 721–741.
262 V. N. Salomone, J. M. Meichtry, G. Zampieri and M. I. Litter, *Chem. Eng. J.*, 2015, **261**, 27–35.
263 P. A. K. Reddy, P. V. L. Reddy, E. Kwon, K.-H. Kim, T. Akter and S. Kalagara, *Environ. Int.*, 2016, **91**, 94–103.
264 X. Yang and D. Wang, *ACS Appl. Energy Mater.*, 2018, **1**, 6657–6693.
265 B. Ai, M. Luo and I. Khan, *Processes*, 2023, **11**, 1398.
266 I. Bolognino, R. Pelosato, G. Marci and I. Natali Sora, *Molecules*, 2023, **28**, 3807.
267 M. Humayun, A. Bahadur, A. Khan and M. Bououdina, *Catalysts*, 2023, **13**, 907.
268 Y.-Y. Lin, P.-H. Lu, F.-Y. Liu, C.-S. Lu and C.-C. Chen, *Catalysts*, 2023, **13**, 812.
269 J. Wang, N. Li, Y. Tang, Y. He and K. Shan, *Int. J. Electrochem. Sci.*, 2022, **17**, 22081.
270 X. Hu, Y. Xu, J. Wang, J. Ma, L. Wang and W. Jiang, *Chem. Eng. J.*, 2023, **451**, 139031.
271 X. Feng, H. Ju, T. Song, T. Fang, W. Liu and W. Huang, *ACS Sustainable Chem. Eng.*, 2019, **7**, 5152–5156.
272 G. Gao, Q. Xi, H. Zhou, Y. Zhao, C. Wu, L. Wang, P. Guo and J. Xu, *Nanoscale*, 2017, **9**, 12032–12038.
273 E. Fan, H. Xu, S. Sun, C. Huang, M. Li, B. Fan, G. Shao, W. Liu, H. Wang, H. Lu and R. Zhang, *Colloids Surf., A*, 2023, **669**, 131510.
274 X. Jia, C. Liu, X. Xu, F. Wang, W. Li, L. Zhang, S. Jiao, G. Zhu and X. Wang, *RSC Adv.*, 2023, **13**, 19140–19148.
275 R. Sun, X. Yu, J. Chen, W. Zhang, Y. Huang, J. Zheng and Y. Chi, *Anal. Chem.*, 2022, **94**, 17142–17150.
276 Y. Zhao, H. Shi, X. Hu, E. Liu and J. Fan, *Chem. Eng. J.*, 2020, **381**, 122692.
277 Y. Zhao, Y. Xu, X. Jing and W. Ma, *Food Chem.*, 2023, **412**, 135420.
278 S. Sharma, S. K. Mehta, A. O. Ibhadon and S. K. Kansal, *J. Colloid Interface Sci.*, 2019, **533**, 227–237.
279 G. V. S. R. P. Kumar, Y. B. Pydiraju, G. V. Lokesh and U. V. S. Likith, *Water Conserv. Sci. Eng.*, 2023, **8**, 17.
280 E. A. Namikuchi, R. D. L. Gaspar, I. M. Raimundo Jr and I. O. Mazali, *Spectrochim. Acta, Part A*, 2023, **300**, 122915.
281 A. Solinska, J. Marchewka, M. Sitarz and T. Bajda, *Spectrochim. Acta, Part A*, 2023, **299**, 122758.
282 K. Guo, P. Lin, D. Wu, Z. Shi, X. Chen, Y. Han, Y. Tian and X. Li, *Chem.–Eur. J.*, 2023, **29**, e202300400.
283 A. Jimenez-Almarza, A. Lopez-Magano, R. Cano, B. Ortin-Rubio, D. Diaz-Garcia, S. Gomez-Ruiz, I. Imaz, D. Maspoch, R. Mas-Balleste and J. Aleman, *Mater. Today Chem.*, 2021, **22**, 100548.
284 H. Ju, T. Fang, Y. Zhou, X. Feng, T. Song, F. Lu and W. Liu, *Appl. Surf. Sci.*, 2021, **551**, 149452.
285 X.-F. Qi, F. Zhang, Z.-P. Chen, X. Chen, M.-C. Jia, H.-F. Ji and Z.-F. Shi, *J. Mater. Chem. C*, 2023, **11**, 3715–3725.
286 E. D. M. Isa, N. W. C. Jusoh and A. A. M. Rodzi, *Environ. Sci. Pollut. Res.*, 2023, **30**, 116921–116933.
287 Y. Khan, U. Sharafat, S. Gul, M. I. Khan, M. Ismail, M. A. Khan, R. Younus and S. B. Khan, *Green Process. Synth.*, 2023, **12**, 20228128.
288 F. Yang, X. He, T. Xin, H. Yang, L. Bai, L. Gao and Y. Wang, *Molecules*, 2023, **28**, 3968.
289 P. Nehra, P. S. Rana and S. Singh, *Environ. Sci. Pollut. Res. Int.*, 2023, **30**, 70094–70108.
290 A. Panahi, R. Monsef, E. A. Dawi, A. S. Hussein and M. Salavati-Niasari, *Sol. Energy*, 2023, **258**, 372–382.
291 S. Sharma, P. Jakhar and H. Sharma, *J. Appl. Polym. Sci.*, 2023, **140**, e54038.
292 U. A. A. Yasin, M. M. Ahmed, J. Zhang, Z. Jia, T. Guo, R. Zhao, J. Shi and J. Du, *J. Mater. Sci.*, 2023, **58**, 7333–7346.
293 F. Yousefzadeh, M. Ghanbari, E. A. Dawi and M. Salavati-Niasari, *Arabian J. Chem.*, 2023, **16**, 104904.
294 S. Liu, M. Li, Y. Tang and X. Wen, *J. Alloys Compd.*, 2023, **959**, 170528.
295 S. M. M. Yakout and M. E. E. El-Zaidy, *J. Sol-Gel Sci. Technol.*, 2023, **107**, 417–429.
296 S. S. Ahmed, *J. Nanostruct.*, 2023, **13**, 48–58.
297 K. Balu, E. Chicardi, R. Sepulveda, M. Durai, F. Ishaque, D. Chauhan and Y.-H. Ahn, *Sep. Purif. Technol.*, 2023, **309**, 122998.
298 S. Moradi, M. Farhadian, A. R. S. Nazar and M. Moghadam, *J. Mol. Liq.*, 2023, **377**, 121520.
299 S. Ravikumar, D. Mani, E. Chicardi, R. Sepulveda, K. Balu, V. Pandiyan and Y. H. Ahn, *Ceram. Int.*, 2023, **49**, 9551–9559.
300 A. Moulahi, *J. Inorg. Organomet. Polym. Mater.*, 2023, **33**, 3948–3960.
301 I. Ahmad, M. Muneer, A. S. Khder and S. A. Ahmed, *ACS Omega*, 2023, **25**, 22708–22720.

302 S. Asgari, G. M. Ziarani, A. Badiei, R. S. Varma, S. Iravani and F. Mohajer, *RSC Adv.*, 2023, **13**, 17324–17339.
303 K. Layek, *Catal. Surv. Asia*, 2023, **27**, 349–362.
304 W. Liu, H. Xie, X. Guo, K. Wang, C. Yang, N. Wang and C. Ge, *Opt. Mater.*, 2023, **136**, 113398.
305 P. Li, Z. Wang, S. Yang, G. Lyu, Y. Gu, J. Chen and G. Yang, *Int. J. Biol. Macromol.*, 2023, **242**, 125137.
306 M. Lv, H. Liu, L. He, B. Zheng, Q. Tan, M. Hassan, F. Chen and Z. Gong, *Environ. Res.*, 2023, **231**, 116218.
307 M. Sharma, D. Rajput, V. Kumar, I. Jatain, T. M. Aminabhavi, G. Mohanakrishna, R. Kumar and K. K. Dubey, *Environ. Res.*, 2023, **231**, 116132.
308 D.-E. Lee, S. Moru, K. P. Reddy, W.-K. Jo and S. Tonda, *J. Mater. Sci. Technol.*, 2023, **148**, 19–30.
309 J. Lv, X. Lu, C. Zhou, X. Zeng and Y.-y. Li, *J. Alloys Compd.*, 2023, **960**, 170514.
310 D. Song, M. Li, L. Liao, L. Guo, H. Liu, B. Wang and Z. Li, *Nanomaterials*, 2023, **13**, 1841.
311 Q. Sun, X. Hu, Y. Zhao, J. Zhang and J. Sheng, *Environ. Sci. Pollut. Res.*, 2023, **30**, 75247–75261.
312 D. Cardenas-Morcoso, A. F. Gualdrón-Reyes, A. B. Ferreira Vitoreti, M. García-Tecedor, S. J. Yoon, M. Solis de la Fuente, I. Mora-Seró and S. Gimenez, *J. Phys. Chem. Lett.*, 2019, **10**, 630–636.
313 L. Wang, M. Niu, Y. Liu, Y. Xie, Z. Ma, M. Zhang and C. Hou, *J. Colloid Interface Sci.*, 2023, **645**, 639–653.
314 Y. Xiao, Y. Jiang, E. Zhou, W. Zhang, Y. Liu, J. Zhang, X. Wu, Q. Qi and Z. Liu, *J. Mater. Sci. Technol.*, 2023, **153**, 205–218.
315 J. Xing, J. Huang, X. Wang, F. Yang, Y. Bai, S. Li and X. Zhang, *J. Environ. Manage.*, 2023, **343**, 118210.
316 X. Qian, Z. Chen, X. Yang, W. Zhao, C. Liu, T. Sun, D. Zhou, Q. Yang, G. Wei and M. Fan, *J. Cleaner Prod.*, 2020, **249**, 119335.
317 Y. Zhao, Y. Wang, X. Liang, H. Shi, C. Wang, J. Fan, X. Hu and E. Liu, *Appl. Catal., B*, 2019, **247**, 57–69.
318 P. Wang, X. Diao, X. Zhang, Z. Zhao, H. Gao, J. T. S. Irvine and G. Wang, *Mater. Today Phys.*, 2023, **35**, 101043.
319 X. Wang, J. He, L. Mao, X. Cai, C. Sun and M. Zhu, *Chem. Eng. J.*, 2021, **416**, 128077.
320 M. T. Hoang, C. Han, Z. Ma, X. Mao, Y. Yang, S. S. Madani, P. Shaw, Y. Yang, L. Peng, C. Y. Toe, J. Pan, R. Amal, A. Du, T. Tesfamichael, Z. Han and H. Wang, *Nano-Micro Lett.*, 2023, **15**, 161.
321 A. A. Alothman, M. R. Khan, M. D. Albaqami, S. Mohandoss, Z. A. Alothman, N. Ahmad and K. N. Alqahtani, *Nanomaterials*, 2023, **13**, 3026.
322 S. Das, T. Paul, S. Maiti and K. K. Chattopadhyay, *Mater. Lett.*, 2020, **267**, 127501.
323 A. A. Bhat, S. A. Khandy, I. Islam and R. Tomar, *Sci. Rep.*, 2021, **11**, 16473.
324 A. Asadi, N. Khosroshahi, M. Hosseinpour and V. Safarifard, *Mater. Sci. Semicond. Process.*, 2023, **165**, 107707.
325 Y. Liu and Z. Ma, *Colloids Surf., A*, 2021, **628**, 127310.
326 M. Karami, M. Ghanbari, O. Amiri and M. Salavati-Niasari, *Sep. Purif. Technol.*, 2020, **253**, 117526.
327 G. Yuan, S. Feng, Q. Yang, F. Yi, X. Li, Y. Yuan, C. Wang and H. Yan, *J. Mater. Chem. C*, 2023, **11**, 7570–7574.